



A dynamic 2DH flocculation model for coastal domains

Sebastian Escobar^{1,2} · Qilong Bi^{1,3} · Michael Fettweis⁴ · Samor Wongsoredjo¹ · Jaak Monbaliu¹ · Erik Toorman¹

Received: 31 January 2022 / Accepted: 20 April 2023 / Published online: 15 June 2023
© Springer-Verlag GmbH Germany, part of Springer Nature 2023

Abstract

A dynamic two-dimensional depth-averaged (2DH) parameterization for flocculation of cohesive sediments is proposed based on the kinetic model by Winterwerp (J Hydraul Res 36:309–326, 1998). The aim is to achieve a realistic representation of the suspended sediment field by accounting for flocculation, also taking into consideration its dependence on advection, turbulent diffusion, and turbulent shear. This formulation is evaluated in a sand-mud model of the Belgian Coast and the Western Scheldt. Results indicate that it can reproduce known sediment transport patterns: modelled floc size and suspended sediment concentrations are in the range of measurements. When evaluating the model results spatially, the extent and shape of the coastal sediment plumes are similar to the observed suspended particle matter (SPM) maps from the PROBA-V satellite. Therefore, the use of the presently proposed flocculation model has added value to improve sediment transport calculations in coastal areas.

Keywords Sediment transport · Flocculation · Coastal morphodynamics

1 Introduction

Studies by Lee et al. (2011), Shen et al. (2018), and Shen et al. (2019) showed that size-varying flocs can be modelled through single-class and multiple-class flocculation equations. These allow examining complicated particle-size distributions, predicting better their settling velocities, and can optionally account for biological processes that enhance aggregation or breaking. These models are based on population balance equations (PBE) (Hulburt and Katz 1964; Randolph 1964), on extensive studies of floc density, strength, form, and fractal features (von Smoluchowski 1917; Tambo and Watanabe 1979; Weitz and Oliveria 1984; Maggi et al. 2007), and on flocculation kinetics (Tambo and Watanabe 1984; Dyer 1989; van Leussen 2011). Yet these models are not efficient for application to large-scale coastal studies. The many scales involved and complex interactions between primary particles and their aggregates, plus stability and computational time considerations, make them only applicable to small or idealized geometries like Quasi-1D

vertical frameworks and 3D schematized estuarine domains, or to controlled study cases like mixing tanks and settling column experiments (Bi et al. 2020).

Winterwerp (1998) proposed a flocculation model, which directly calculates the mean floc size assuming that the floc density is proportional to the size to a certain power, similar to fractal theory (Kranenburg 1994; Chapalain et al. 2019). This model is particularly popular, and its use in literature is extensive (Winterwerp 2002; Tarpley et al. 2019; Horemans et al. 2020; Zhang et al. 2020). Authors generally take advantage of its mathematical simplicity because it consists of a single ordinary differential equation, which facilitates its use in idealized estuaries and experiments. However, Kuprenas et al. (2018) found that this model can yield unreasonably large floc sizes when turbulent shear or suspended particle matter (SPM) fall outside of the range of calibration parameters.

It is not uncommon therefore that coastal modelling studies ignore or try to parametrize the flocculation dynamics to get better values of the sediment settling velocity, and thus more realistic SPM results. The most straightforward method is to calibrate the sediments settling velocity, which is taken as a parameter and its values fine-tuned to match SPM time series. However, this process is very subjective and a wide range of settling velocity values are often found in the literature of the same geographical area (Van den Eynde 2018;

Responsible Editor: Sandro Carniel

✉ Sebastian Escobar
s.escobar@hrwallingford.com

Extended author information available on the last page of the article

Bi and Toorman 2015; Cox et al. 2019). Moreover, seasonal variation of the settling velocity is well documented (Fetweis and Baeye 2015; McAnally and Mehta 2000; Maerz et al. 2016; Duy Vinh et al. 2018; Chang et al. 2006), which means that such calibrations should also involve seasonality. Another alternative is the use of empirical settling velocity equations that are a function of hydrodynamics and sediment transport. For example, the Soulsby et al. (2013) formula is a function of the instantaneous turbulent shear and suspended sediment concentration. Satellite data can also be used and assimilated to the settling velocity parameter by algorithms taken from computational science disciplines (Margvelashvili et al. 2013; Wang et al. 2018, 2020). These methods are promising, especially with rapid advances in remote sensing technologies, but they are limited by the temporal frequency of satellite data, and by its sensitivity to cloudiness, and because satellite data only provide information in the water surface.

We propose a comprehensive two-dimensional depth-averaged (2DH) flocculation formulation based on Winterwerp (1998). This model introduces new terms such as turbulent drift to account for the relative velocity of the sediment fraction to the flow, turbulence inertia correction, which emulates turbulence growth and decay rates, and data-based modifications of the breaking source term. The aim is to achieve a model that can deal with the many across-scales exchanges of mass and energy happening in the coastal zone (e.g., throughout offshore, nearshore, inter-tidal zones, and between the bed and the water column), along with floc-scale processes. Lastly, this flocculation model is assessed in a real setup of the Belgian Coast by comparison with field and satellite data.

2 Materials and methods

2.1 Model formulation

The following kinetic model for tracking the evolution of the floc size is proposed:

$$\frac{\partial d}{\partial t} + (u + u_D) \frac{\partial d}{\partial x} + (v + v_D) \frac{\partial d}{\partial y} = A - B \quad (1)$$

t is the independent time variable, d is the mean floc size, u and v are the depth-averaged velocity components along x and y directions, and A and B are the aggregation and breakage source terms.

This model accounts for the dispersive velocity of floc particles through the turbulent drift (u_D , v_D), which is obtained

from the turbulent mass flux term in the sediment mass balance equation:

$$\begin{pmatrix} u_D \\ v_D \end{pmatrix} = -\frac{1}{C} \frac{\nu_t}{\sigma} \nabla C \quad (2)$$

C is the total mass concentration of the suspended sediment, ν_t the eddy viscosity, and σ the turbulent Schmidt number. Usually, the sediment diffusivity is assumed equal to the turbulent eddy viscosity, and thus the Schmidt number is taken as 1. Nevertheless, studies by Toorman (1997) and Toorman et al. (2002) indicate that a value of 0.7 produces better results for high-turbidity flows based on the work by Turner (1973).

Different from the original work by Winterwerp (1998), in this formulation, the influence of volumetric concentration (ϕ) on the breakage term (B) is considered. This follows observations by Manning and Dyer (1999) that point to a negative correlation of the sediment concentration with floc size.

$$\begin{aligned} A &= k_a \phi d^{(4-n_f)} G \\ B &= k_b \phi \frac{(d - d_p)^{(3-n_f)}}{d_p} d^2 G^{3/2} \end{aligned} \quad (3)$$

G is the turbulent shear rate, and d_p the primary particle, defined as the smallest possible particle size of the clay units, which are compact microflocs of the order of 10 to 20 μm in size (based on LISST data, Sect. 2.2.2). n_f is the pseudo-fractal dimension of the sediment particles' population; k_a and k_b are calibration constants.

Flocs undergo changes in their structure, strength, composition, and electrolyte concentration as their size changes (Chakraborti et al. 2003; Khelifa and Hill 2006; Maggi et al. 2007; Son and Hsu 2009). Therefore, the flocs' population pseudo-fractal dimension, rather than constant, is to be considered a function of the floc size. Following this reasoning, a formula similar to the one proposed by Maggi et al. (2007) is used:

$$n_f = n_{max} \left(\frac{d}{d_p} \right)^{-\beta} \quad (4)$$

$n_{max} = 2.5$ is the maximum pseudo-fractal dimension corresponding to microflocs (the strongest basic aggregates found in the environment, which rarely break up into primary clay particles), and the parameter $\beta = 0.09$, based on observed mean flocs sizes of micro-, macro-, and megafloc populations in the Belgian coastal area (Lee et al. 2012).

The turbulent shear rate is usually defined as $G = \sqrt{\frac{\epsilon}{\nu}}$, with ϵ being the turbulence kinetic energy dissipation, and

ν the fluid kinematic viscosity (Saffman and Turner 1956). For applications with turbulence models different from the $k - \epsilon$, such as this work, Toorman (2020) proposed the following formula based on extrapolation of direct numerical simulations data:

$$G = \frac{1}{2} \frac{u_*^2}{\nu} \tag{5}$$

Where $u_* = \sqrt{\tau_b/\rho_w}$ is the friction velocity, τ_b the bed shear stress, and ρ_w the water density. Note that with this formula the shear rate is computed at the vicinity of the bed level, where u_* and τ_b occur.

Equation (5) implies that G becomes 0 when $u_* = 0$ m/s. In reality, there always remains turbulence in the water column because of the inertia of the dissipation. To account for this memory effect, Toorman (2020) proposes the relaxation equation:

$$G = G_{eq} + (G_{t-\Delta t} - G_{eq})exp(-\Delta t/T_r) \tag{6}$$

Where G_{eq} is the turbulent shear rate calculated with Eq. (5), $G_{t-\Delta t}$ is the turbulence shear rate at a previous time step, and T_r is the relaxation time parameter, to be calibrated based on the time lag between shear rate and suspended sediment concentration peaks.

In addition to the flocculation model, the settling velocity is modified from Dietrich (1982) formula to be valid over a wider range of particle Reynolds numbers (Toorman 2022).

$$\begin{aligned} \log\left(\frac{w_s}{w_0}\right) &= b_2(\log(1 + d_*))^2 \\ &+ b_3(\log(1 + d_*))^3 + b_4(\log(1 + d_*))^4 \\ d_* &= (g'/\nu^2)^{1/3}d \\ g' &= (\rho_f/\rho_w - 1)g \\ \rho_f &= \rho_w + (\rho_s - \rho_w)\left(\frac{d}{d_1}\right)^{n_F-3} \\ w_0 &= g'd^2/18\nu \end{aligned} \tag{7}$$

Where $b_2 = -0.33$, $b_3 = -0.056$, and $b_4 = 0.018$ are empirical constants, d_* the non-dimensional mean floc diameter, and g' is the specific gravity of sediment particles. ρ_f and ρ_s are respectively the floc bulk and the dry sediment density, g the gravity acceleration, w_s the settling velocity of the sediment, and w_0 the Stokes settling velocity (theoretically characteristic of spherical particles settling with very small Reynolds numbers).

2.1.1 Numerical solution

A MATLAB implementation of Eqs. (1) to (7) was used to prove the model’s functioning on simplified cases. This con-

sisted of a solver for a single zero-dimensional point that receives input shear rate and concentration signals, and outputs the mean floc size after solving Eq. (1). The solution of (1) is based on Press et al. (1992) 4th-order step-varying Runge–Kutta algorithm, which adjusts the timestep between 0.5 and 5 s depending on the temporal rate of change of the mean floc size. The reason for using this solver is that the source terms in (3) have many time-varying inputs (e.g., the instantaneous floc size, the turbulent shear rate, and the volumetric sediment concentration) which can be subject to abrupt changes. Furthermore, non-stiff ODE solvers (e.g., Euler, or a constant step Runge–Kutta method) can easily become unstable under these conditions. For a pair of input turbulent shear rate and sediment concentraion signals, the solution steps are:

1. Calculate the pseudo-fractal dimension (4).
2. Calculate the instantaneous value of the aggregation and breakage source terms (3).
3. Solve Eq. (1) numerically with the Press et al. (1992) algorithm.

The results (Fig. 1) show the expected pattern where aggregation takes place during low shear, and breakage during high shear. Also, they show the modulation of the shear rate caused by (6). A more realistic test was carried out using measurements from the MOW1 station as input data (see Section 2.2.2). This is shown in Fig. 2; the model equations reproduce the growth and breakage phases of microflocs and macroflocs (20 to 200 μ m), and it does not match the largest measured particles, which even grow larger than the scale of the LISST measurements. But these may be biological megaflocs, loose structures of minerals and phytoplankton, or phytoplankton aggregates, because the data was taken are during the spring, which is the diatom growing season (Nohe et al. 2020). Further, these megaflocs occur more frequently during lower tidal amplitudes (18–19/04/2009) than at the beginning of the time series.

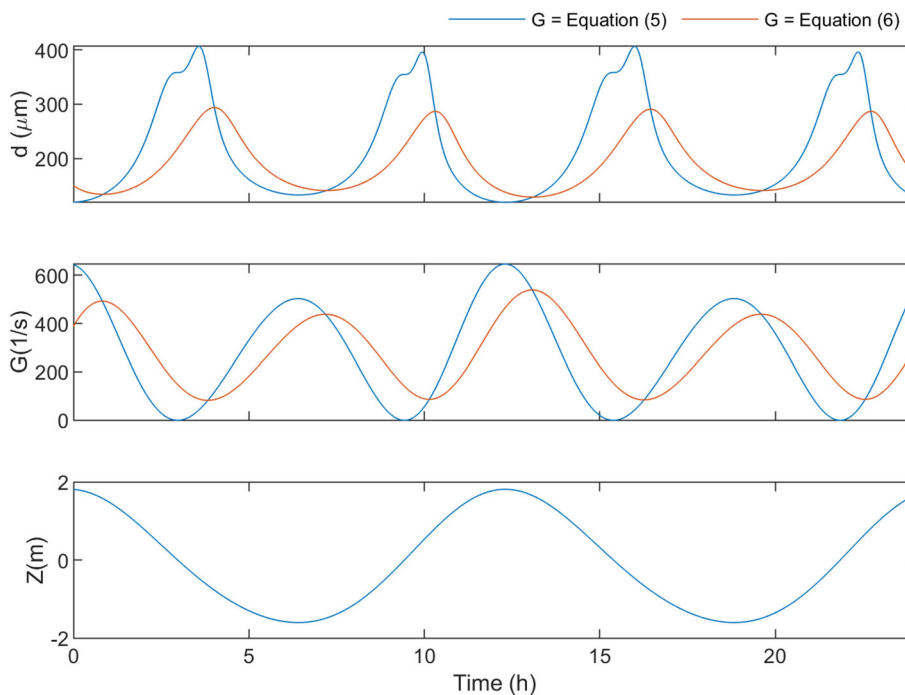
2.2 Application: the Belgian Coast

Having tested the model in simplified conditions, the next step is using the newly formulated flocculation model in a more realistic model of the Belgian Coast.

2.2.1 Study area

The study area covers the Belgian Coast and the Western Scheldt (Fig. 3). Water-depth values range from 0 to 30 m, the bottom topography consists of sandbanks (e.g., Wenduine bank and Paardenmarkt), beaches, tidal flats, shoals (e.g., Vlakte van de Raan, Rassen and Bankje van het Zouteland), and tidal channels in the foreshore and within the Western

Fig. 1 Flocculation model results for a synthetic input tide signal (third row). These results were obtained with parameters $k_a = 1600$, $k_b = 60$, $d_p = 10\mu\text{m}$, $\phi = 0.003\text{ ml/m}$, $n_{max} = 2.5$, and $\nu = 1.E - 6\text{ m}^2/\text{s}$. $Tr = 3600.0\text{ s}$. The shear velocity, not shown in the figure but used to calculate G , is estimated with Nikuradse friction law assuming a roughness height of $k_s = 0.03\text{ m}$

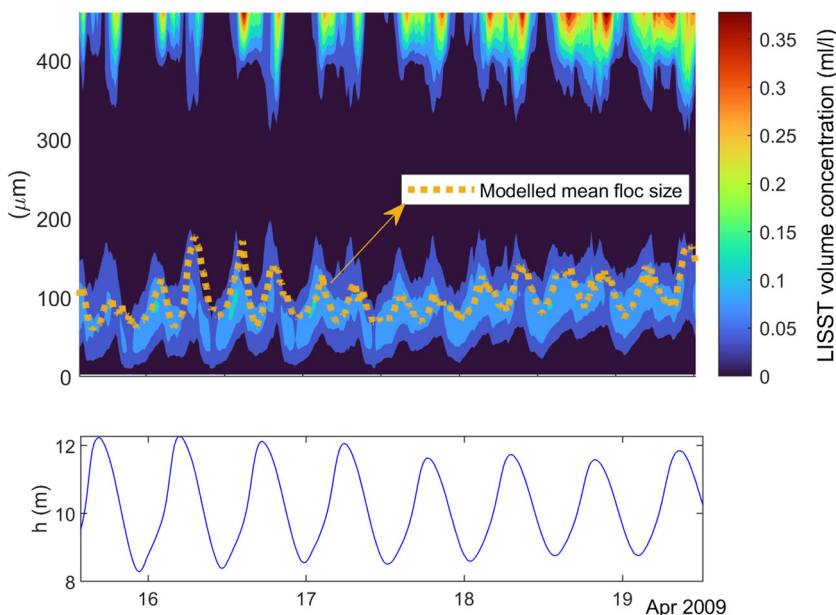


Scheldt estuary. Near the port of Zeebrugge is situated a coastal turbidity maximum area with SPM concentrations between 0.1 g/l and more than 3 g/l near the bed (Baeye et al. 2011; Fettweis et al. 2012). Studies by Baeye et al. (2012) around this area revealed bed boundary level changes of up to 0.2 m during spring-neap tide cycles, suggesting the occurrence of lutoclines and possibly of fluid mud layers.

Tides of the Belgian Coast are of the semi-diurnal type, with approximately two high and low water cycles per day.

The maximum tidal range is 4.8 m during spring tide and 3.1 m during neap tides. Offshore, the predominant harmonic constituent is M2 (principal lunar). The harmonic constituent S2 (principal solar) is also relevant because its superposition with M2 causes spring-neap cycles approximately every 15 days. The nearshore tidal current ellipses are elongated and vary between 0.2 and 0.8 m/s during spring tide and 0.2 and 0.5 m/s during neap tide at 2 m above the bed. The large tidal range and the low freshwater discharges result in a well-mixed water column (Fettweis et al. 2016; Brand et al. 2019).

Fig. 2 Flocculation model results compared with LISST-measured floc volume concentration at the MOW1 station. These results were obtained with parameters $k_a = 1800$, $k_b = 20$, $d_p = 20\mu\text{m}$, $n_{max} = 2.5$, and $\nu = 1.E - 6\text{ m}^2/\text{s}$. G , not shown in the figure, calculated from velocity measurements and assuming a Nikuradse friction law with a roughness height of $k_s = 0.03\text{ m}$



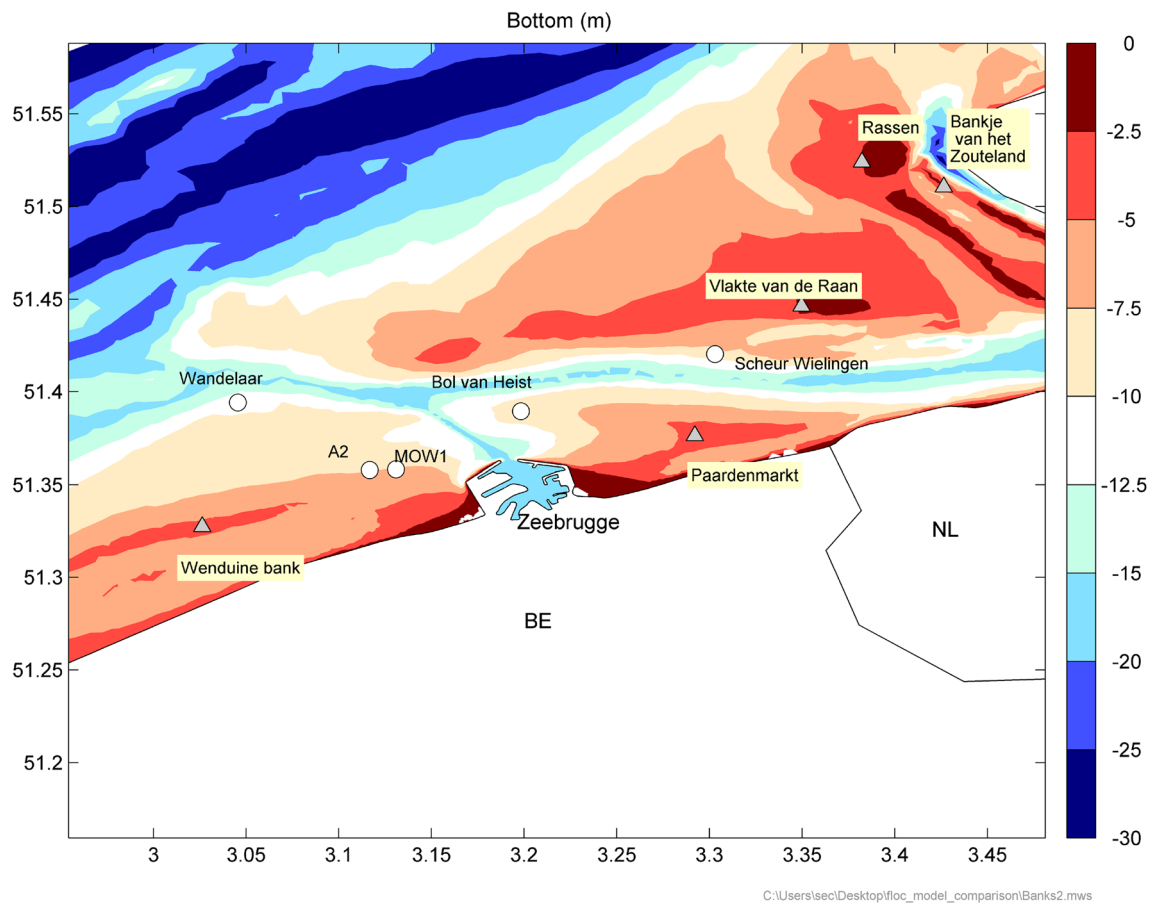


Fig. 3 Study area. The color contours show the water depth below mean sea level in m. Circle markers show the position of measurement stations, and the triangles indicate the position of known banks and shoals

The most frequent waves along the Belgian Coast, occurring approximately 30% of the time, propagate almost parallel to the shoreline, with north-east direction, a time-averaged significant wave height of 0.8 m, and a typical wave period of about 6 s.

2.2.2 Available data for calibration and validation

Data from the Flemish banks monitoring network (Meetnet Vlaamse Banken) was used for the assessment of modelled free surface water levels, flow velocities, significant wave height, and mean wave period.

Current velocity and SPM concentration were collected with a tripod at station MOW1 (Fig. 3). The instrumentation suite consisted of a point velocimeter (5-MHz ADVOcean velocimeter), a downward-looking ADP profiler (3 MHz SonTek Acoustic Doppler Profiler), and a Sequoia LISST-100X, used to measure the particle size distribution and volume concentration. The data were collected every 15 min for the LISST, and ADV, while the ADP was set to record a profile every 1 min; later on, averaging was performed to a 15-min interval (Fettweis et al. 2019).

Spatial information from the PROBA-V satellite mission was also used with the purpose of validation. This data are surface SPM concentration maps retrieved by Knaeps et al. (2017).

Modelled concentration results are brought to the reference level of the measurements and the satellite data with the Van den Eynde (2018) conversion algorithm.

2.3 Implementation in the TELEMAC modelling system

The setup consists of a layered array of nested meshes (Fig. 4) that run in the TELEMAC software (Hervouet 2000). The largest mesh (in spatial extension) covers the North Sea (NSG) and simulates hydrodynamics (waves and currents). Smaller meshes, nested in the NSG model, cover the Belgian Coast and the Western Scheldt (BCG). These smaller meshes take their seawards boundary conditions (depth, current velocity, and directional spectra of wave action) from the NSG model. This setup is inspired in modelling studies by Van den Eynde (2018); Komijani and Ortega (2016); Zhang et al. (2020).

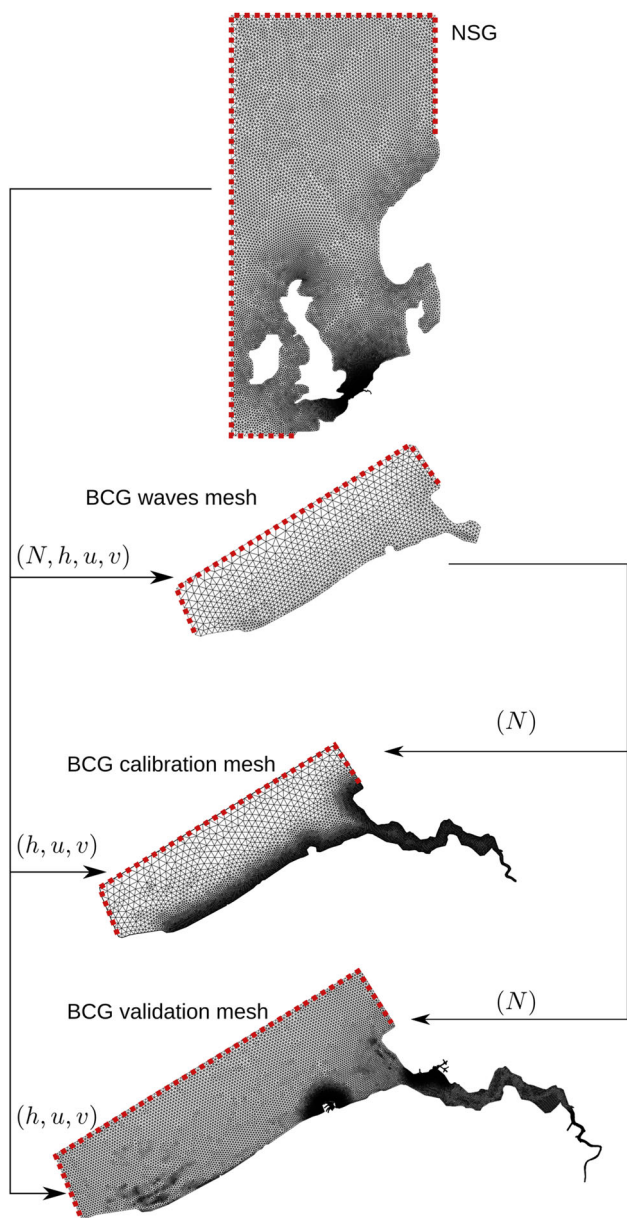


Fig. 4 Mesh layering of the North Sea and the Belgian Coast models. The dashed red lines indicate the models’ offshore open boundaries. The North Sea (NSG) provides boundary directional spectra of wave action (N), the boundary depth (h), and boundary flow velocities (u, v) for meshes of the Belgian Coast (BCG). Different meshes of the Belgian Coast are used for wave calculations, for calibration of parameters, and for validation

The NSG and BCG models’ timesteps are 5 s, with a coupling period of 300 s for the waves module (Sect. 2.3.2). The NSG has 20,603 nodes with edge lengths between 90 and 900 m. The BCG mesh used during calibration has 8633 nodes (edge lengths from 321.5 to 6.2 km). The BCG mesh used during validation has 24,394 nodes (67.9 to 2.0 km edge lengths). A differential approach is used for speeding up the waves calculation on the BCG model (Breugem et al. 2019);

thus, the BCG mesh of the waves module (see Section 2.3.2) has only 5434 nodes (edge lengths between 321.5 and 6.2 km) and excludes the Western Scheldt part of the study area. To minimize any transient effects of these initial conditions, a warming up time of 25 days was simulated and only the results after this period are considered for analysis.

Free surface elevation of the NSG model is prescribed from the TPX08 global tides database (Dushaw et al. 1997). It considers eight primary (M2, S2, N2, K1, O1, P1, Q1), two long period (Mf, Mm), and three non-linear (M4, MS4, MN4) harmonic constituents. The initial hydrodynamics conditions are set to zero flow velocity and water level throughout the domain. The wave boundary conditions of the NSG model are based on a spectrum discretized in 12 directions and 25 frequencies following the discretization function $f_n = f_1 q^{n-1}$, with minimal frequency $f_1 = 0.04$ Hz and frequential ratio $q = 1.1007$. Horizontal wind velocities are interpolated spatially (inverse distance weighting) and temporally (linear) from the ECMWF ERA-Interim dataset (Berrisford et al. 2009). The boundary condition for the NSG model is a zero spectrum of wave action, and for the BCG model the boundary spectrum is imposed from results of the NSG model; thus, the same spectral discretization is used. The boundary condition at the sediment bed, for all models run during this work, is the dynamic friction law Bi and Toorman (2015).

The bathymetries of these meshes were generated from multiple datasets: The NSG uses data from EMODNET (Thierry et al. 2019) and the BCG model is made of data collected during the NEVLA project (Maximova et al. 2009). Along the foreshore, the data belongs to AMDK (2017), and on the western boundary of the model, we used data from SHOM (2015). The vertical datum of all grids is the mean sea level.

2.3.1 Hydrodynamics module

Hydrodynamics are computed by the TELEMAC-2D module which solves the shallow water equations of continuity (8) and momentum balance (9, 10) (Hervouet 2000).

$$\frac{\partial h}{\partial t} + \frac{\partial(hu)}{\partial x} + \frac{\partial(hv)}{\partial y} = 0 \tag{8}$$

$$\frac{\partial hu}{\partial t} + u \frac{\partial hu}{\partial x} + v \frac{\partial(hv)}{\partial y} = -g \frac{\partial Z}{\partial x} + F_x + \frac{1}{h} \nabla \cdot (hv_t \nabla u) \tag{9}$$

$$\frac{\partial hv}{\partial t} + u \frac{\partial hu}{\partial x} + v \frac{\partial(hv)}{\partial y} = -g \frac{\partial Z}{\partial y} + F_y + \frac{1}{h} \nabla \cdot (hv_t \nabla v) \tag{10}$$

h is the water depth, g is the gravity acceleration, Z the elevation of the free water surface, F is a source term that encompasses wind (Flather 1979), Coriolis, and the time-space varying friction induced forces. From Bi and Toorman (2015) friction law, we calculate time-space-varying bed

roughness and bed shear stress directly from the hydrodynamics with a Nikuradse roughness height of 0.03 m.

The turbulent eddy viscosity (ν_t) is modelled with the Smagorinsky formulation:

$$\begin{aligned} \nu_t &= C_{s2} \Delta_{xy}^2 (2\bar{S}\bar{S})^{1/2} \\ \bar{S} &= \frac{1}{2} \left(\frac{\partial u}{\partial y} + \frac{\partial v}{\partial x} \right) \end{aligned} \tag{11}$$

with $C_{s2} = 0.01$, \bar{S} is rate of strain tensor, and Δ_{xy} is the spatial grid size.

2.3.2 Waves module

Evolution of the directional spectrum of wave action (12) is calculated in TOMAWAC (Benoit et al. 1997; Breugem et al. 2019).

$$\frac{\partial N}{\partial t} + \dot{x} \frac{\partial N}{\partial x} + \dot{y} \frac{\partial N}{\partial y} + \dot{k}_x \frac{\partial N}{\partial k_x} + \dot{k}_y \frac{\partial N}{\partial k_y} = Q(x, y, k_x, k_y, t) \tag{12}$$

N is the wave action density, k_x and k_y wave number vector components along the x and y directions respectively, and Q the source terms (e.g., wind-driven wave generation, whitecapping, bottom friction, wave breaking). The dot over the variables denotes the time transfer rates of each variable that are given by the linear wave theory; more details can be found in the TOMAWAC user manual (Fouquet 2020).

In this work, the following processes are taken into account: wind-driven wave generation (Komen et al. 1996), white-capping dissipation (Komen et al. 1984), bottom friction (Hasselmann et al. 1973), quadruplet interactions (Hasselmann et al. 1985), and depth-induced breaking (Batjes and Janssen 1978).

2.3.3 Sediment transport module

Suspended sediment concentration and bed evolution are calculated in the GAIA module (Tassi et al. 2023), with the advection–diffusion (13) and Exner (14) equations. We assumed that the sediment suspension can be characterized by two sediment classes. One sediment class is sand with constant grain size of 200 μm , and the other is a cohesive sediment fraction with variable mean floc diameter calculated with Eq. (1). Both sand and mud classes can be transported via the suspended load, and their mass concentrations are

Algorithm 1 Erosion law.

if $f_m < f_{m,s}$ then

$$\begin{aligned} \tau_{ce} &= \tau_{ce,s} + x_1 f_m \\ E_s &= E_{0s}(1 - f_m) \left(\frac{\tau_b}{\tau_{ce}} - 1 \right)^a \\ E_m &= E_{0s} f_m \left(\frac{\tau_b}{\tau_{ce}} - 1 \right)^a \end{aligned} \tag{16}$$

else if $f_m > f_{m,m}$ then

$$\begin{aligned} \tau_{ce} &= \tau_{ce,m} \\ E_s &= E_{0m}(1 - f_m) \left(\frac{\tau_b}{\tau_{ce,m}} - 1 \right) \\ E_m &= E_{0m} f_m \left(\frac{\tau_b}{\tau_{ce,m}} - 1 \right) \end{aligned} \tag{17}$$

else

$$\begin{aligned} \tau_{ce} &= \frac{\tau_{ce,s} + x_1 f_{m,m}}{f_{m,m} - f_{m,s}} (f_{m,m} - f_m) + \frac{f_m - f_{m,s}}{f_{m,m} - f_{m,s}} \tau_{ce,m} \\ E_s &= (1 - f_m) \left(E_{0s} + \frac{(f_m - f_{m,s})(E_{0m} - E_{0s})}{f_{m,m} - f_{m,s}} \right) \\ &\quad \left(\frac{\tau_b}{\tau_{ce}} - 1 \right)^{\left[a + \frac{1-a}{f_{m,m} - f_{m,s}} - (f_m - f_{m,s}) \right]} \\ E_m &= f_m \left(E_{0s} + f_m \frac{(f_m - f_{m,s})(E_{0m} - E_{0s})}{f_{m,m} - f_{m,s}} \right) \\ &\quad \left(\frac{\tau_b}{\tau_{ce}} - 1 \right)^{\left[a + \frac{1-a}{f_{m,m} - f_{m,s}} - (f_m - f_{m,s}) \right]} \end{aligned} \tag{18}$$

end if

$\triangleright E$ is the erosion flux, The variable f defines the sediment class fraction, E_0 is the Partheniades constant, and the subindexes s and m denote sand and mud particle classes respectively. $f_{m,s} = 30\%$ and $f_{m,m} = 50\%$ are respectively the thresholds for non-cohesive and cohesive regimes of erosion. $\tau_{ce,s}$ and $\tau_{ce,m}$ are the critical shear stress for erosion of sand and mud respectively. $x_1 = 0.5 \text{ N/m}^2$, per (Bi and Toorman 2015).

solved with (13).

$$\frac{\partial C_j}{\partial t} + (u, v) \cdot \nabla C_j = \epsilon_s \nabla^2 C_j + \frac{E_j - D_j}{h} \tag{13}$$

$$(1 - n) \frac{\partial Z_f}{\partial t} + \nabla \cdot Q_s = \frac{\sum D_j - E_j}{\rho_s} \tag{14}$$

The index j notes the sediment class, and $\epsilon_s = \nu_t / \sigma$ is the sediment diffusivity, with σ the turbulent Schmidt number taken as 0.70, as in (2). E and D are the erosion and deposition fluxes. n is the sediment bed porosity, Z_f is the elevation of the bed, and Q_s is the bedload transport rate of sand.

The bed shear stress (τ_b) of the combined wave-current field was computed with the Soulsby and Clarke (2005) formula. The deposition flux (15) was calculated using the

suspension capacity theory by Toorman (2000, 2003), and the erosion flux (Algorithm 1) with a hybrid erosion law proposed by Waeles et al. (2007); Le Hir et al. (2011), and adapted by Bi and Toorman (2015), which empirically combines three erosion regimes: sandy bed, mixed bed, and muddy bed.

$$D_j = w_s C_j \max \left\{ 0, 1 - \frac{\tau_b U R_{fL}}{(1 - \rho_w / \rho_f) g h w_s C_j} \right\}$$

$$R_{fL} = \frac{0.25}{1 + \left(\frac{0.1 u_*}{w_s} \right)^2} \quad (15)$$

w_s is the sediment settling velocity solved with Eq. 7, U is the norm of the flow velocity vector, and R_{fL} is the flux

Richardson number, assuming the sediment suspension is saturated (Toorman 2000).

Initial conditions are a mean floc diameter of $40 \mu\text{m}$ throughout the domain, the winter average surface SPM concentration map from Fettweis et al. (2007), and the relative sand content from maps of Rijkswaterstaat (Ministry of Infrastructure and Water Management, the Netherlands), RBINS-MUMM (Scientific Service Management Unit of the Mathematical Model of the North Sea, Belgium) and Stephens and Diesing (2015). The initial sediment bed is assumed to have two vertical layers with a thickness of 0.1 m and 0.3 m respectively. Boundary conditions offshore are free tracer flux for the suspended concentration of sand, mud, and the floc size variables.

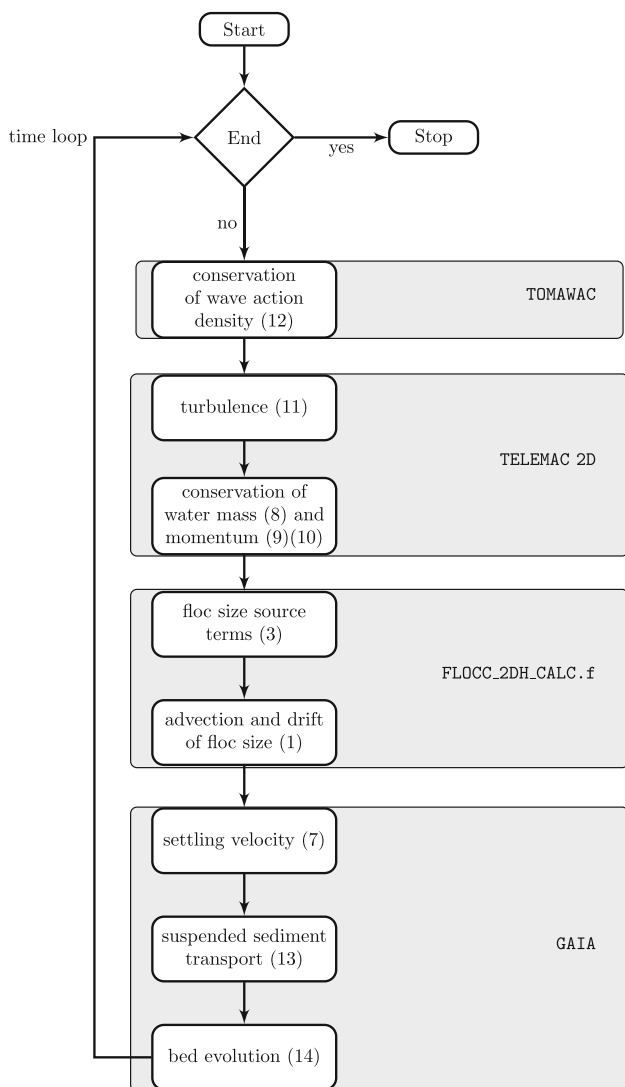


Fig. 5 Computational loop in TELEMAC. The proposed flocculation model has been coded in a new subroutine (FLOCC_2DH_CALC.f) of the TELEMAC software

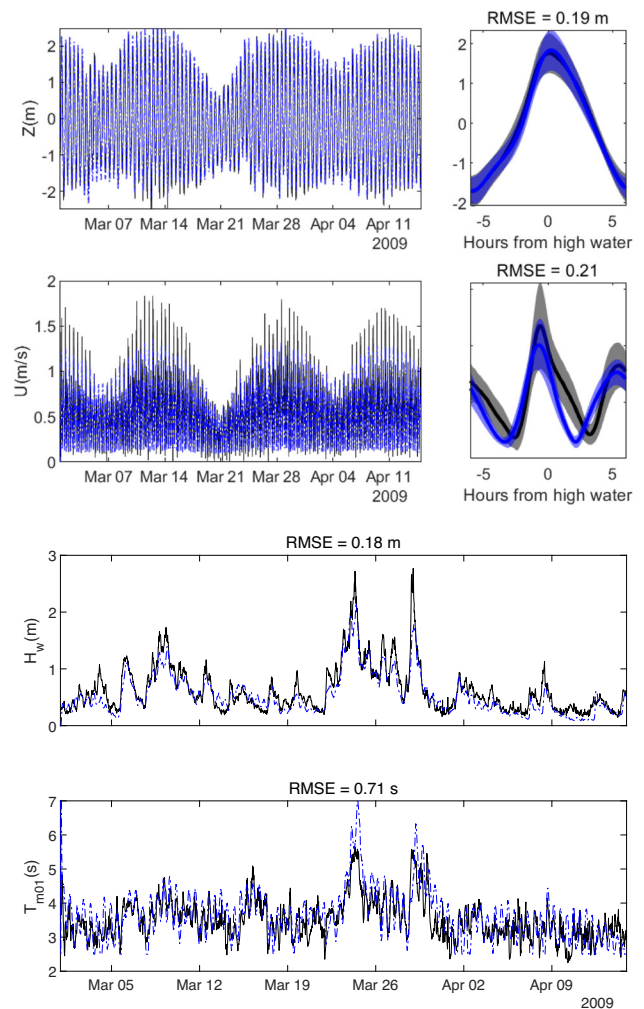
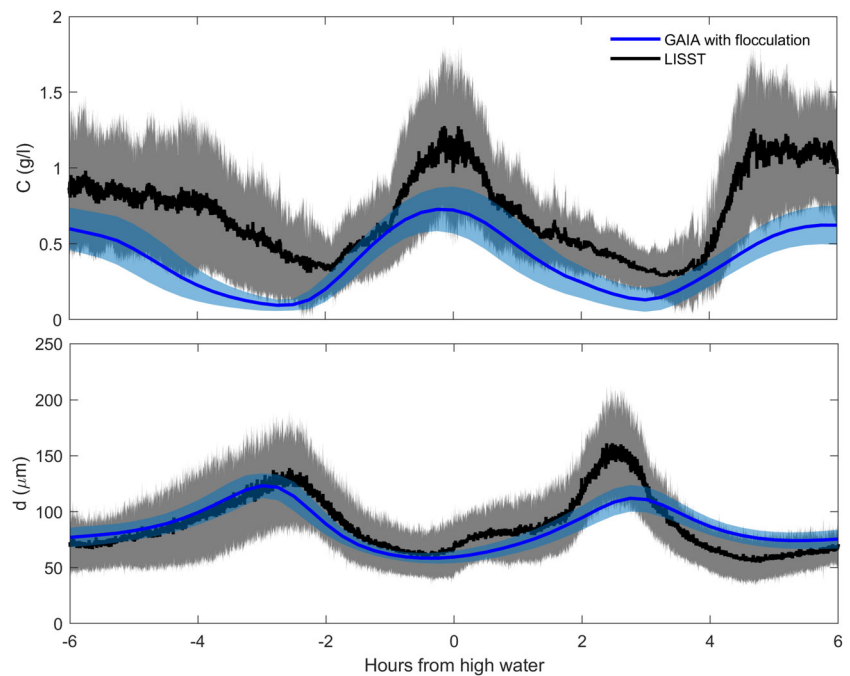


Fig. 6 Hydrodynamics at Bol Van Heist station. The black solid lines are measurements from the Flemish Banks Monitoring Network, and the blue lines are results from the BCG model. In the ensemble averages (first and second rows, right column), the solid lines are temporal means and the shaded areas are the standard deviation

Fig. 7 Model calibration. The black and blue colors represent LISST-measured and modelled values respectively. The lines correspond to the time mean of the data and the shaded areas represent the standard deviation. The data belongs to a time interval from 01/03/2009 to 20/04/2009 at the MOW1 station



2.4 Computational loop in TELEMAC

Equations (1) to (7) were coded in a new subroutine of TELEMAC called FLOCC_2DH_CALC.f. The computational loop is in Fig. 5, subroutine FLOCC_2DH_CALC.f is called after the solution of the flow variables in TOMAWAC and TELEMAC 2D, and before the solution of the suspended sediment transport in the GAIA module. Due to the source terms stiffness, time integration is done through the 4th order step-variable Runge–Kutta method designed and implemented in FORTRAN by Press et al. (1992).

3 Results

3.1 Model calibration

Hydrodynamics Modelled free surface levels and flow velocities agree with the available measurements. Figure 6 (first and second rows) shows that the error is a small fraction of the range of variation of the free surface level and the flow velocities. The root mean square error (RMSE) is 0.19 m for the water level, and 0.21 m/s for the flow velocity. Wave model results (Fig. 6, third and fourth rows) are also acceptable with RMSE values of 0.18 m and 0.71 s for the significant wave height and the mean wave period respectively.

Comparison of modelled hydrodynamics and measurements at other locations yielded similar results. These can be seen in Appendix 2.

Suspended sediment concentration and mean floc diameter

Modelled suspended sediment concentration and mean floc diameter were compared with field data from the MOW1 station. The comparison period spans between 01/03/2009 and 20/03/2009, and the time information was clustered over one high-low-water cycle to facilitate visualization. Figure 7 shows the best fitting model results after calibration (see

Table 1 Parameter values of the calibrated model Belgian Coast model

Parameter	Value
time step (Δt)	5 s
Top layer thickness	0.1 m
Bottom layer thickness	0.3 m
Top layer mud concentration	680.0 kg/m ³
Bottom layer mud concentration	900.0 kg/m ³
E_{0s}	0.008 kg/m ² /s
E_{0m}	0.002 kg/m ² /s
$\tau_{ce,s}$	0.05 N/m ²
$\tau_{ce,m}(1)$	0.02 N/m ²
$\tau_{ce,m}(2)$	0.04 N/m ²
d_p	20 μ m
k_a	1800
k_b	30
T_r	3600 s

$\tau_{ce,m}(1)$ and $\tau_{ce,m}(2)$ are the critical bed shear stresses for erosion of mud for the top and bottom sediment layers respectively

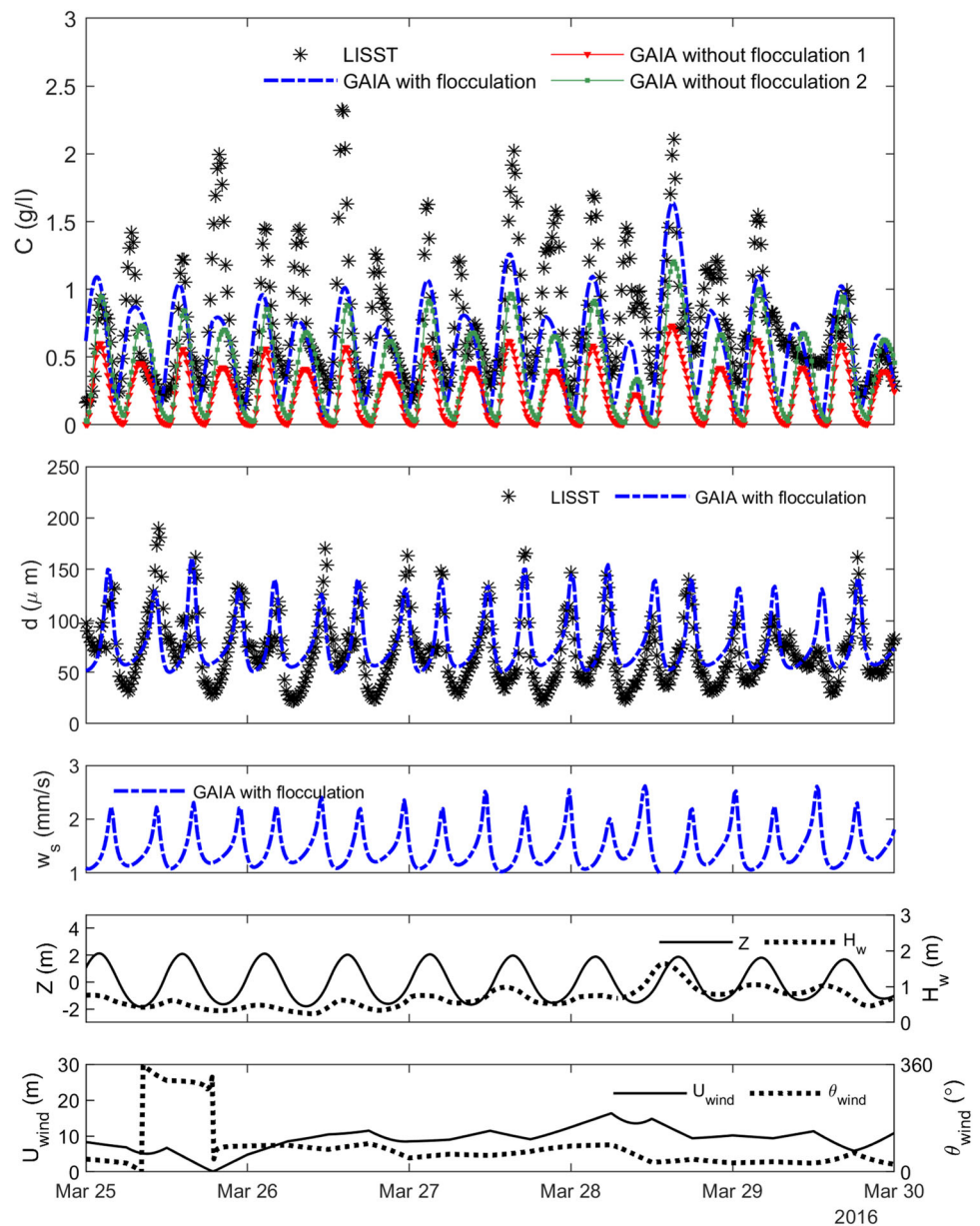
Appendix 1), which were obtained with the parameter values listed in Table 1.

Based on Fig. 7 (first row), the sediment model has a moderate success at reproducing the suspended sediment concentration. Results peak during flood and ebb, and concentration troughs take place during slack waters. This pattern is consistent with the measured data. However, in quantitative terms, the model results underestimate the measurements. Modelled concentrations do not reach neither the same peaks (1.26 g/l during flood, and 1.10 g/l during ebb), nor the same troughs (0.38 g/l and 0.28 g/l during slack waters from low to high and from high to low water respectively). Also, the sediment model has a phase lead of approximately

20 min during ebb, and 1 h during slack waters. The RMSE obtained for the suspended sediment concentration is 0.29 g/l.

The floc size dynamics in Fig. 7 (second row) show that the flocculation model results overlap with the measured mean floc size. Modelled and measured data are within the band of macroflocs and megaflocs (Fettweis et al. 2012; Shen et al. 2018), with values ranging between 70 and 150 μm for the measurements, and 40 to 290 μm for the simulations. Also, the model qualitatively follows the same temporal pattern as the measurements, displaying two peaks within a tidal cycle, one at slack water from ebb to flood, and a higher peak at slack from flood to ebb. The difference between the two floc size peaks is explained by tidal asymmetry, which causes

Fig. 8 Validation of model results. Top row, LISST-measured SPM concentration (black star markers) and modelled suspended sediment concentrations with flocculation (blue line), without flocculation and constant values of $w_s = 3.5$ m/s and $w_s = 2.0$ m/s (green and red lines respectively). Second row, LISST-measured mean floc size and modelled mean floc diameter. Third row, modelled free surface level (solid line) and significant wave height (dashed line). Fourth row, wind speed and direction (trigonometric convention) 10 m above the mean sea level. The simulation “GAIA with flocculation” uses the flocculation formulation proposed in this work. The simulation “GAIA without flocculation 1” assumed a constant settling velocity of 3.5 mm/s, and “GAIA without flocculation 2” assumed a constant settling velocity of 2.0 mm/s



flow velocities—and turbulent shear—to be higher from ebb to flood than in the transition from flood to ebb (Bolle et al. 2010). Model deviations are generally a phase-lead, which causes floc size peaks to happen approximately 40 min earlier than in measurements, plus gaps in amplitude up to 100 μm . The RMSE obtained for mean floc diameters was 23 μm .

3.2 Model validation

Comparison with field data The validation period spans between 20/03/2016 and 30/03/2016. The modelled sediment concentration (Fig. 8, first row) matches in time with the measurements. The model follows the current-driven concentration peaks, although it deviates between 24/03/2016 and 29/03/2016, when U_{wind} is high (up to 15 m/s, see Fig. 8 fifth row) and the effect of waves becomes more important (Fig. 8, fourth row). Figure 8 also shows the results obtained without activating the flocculation equations, and with constant settling velocities of 3.5 mm/s and 2 mm/s (Fig. 8, first row), values previously used by Van den Eynde (2018). Without flocculation the concentration magnitudes are smaller, even showing nil concentrations throughout the totality of the ebb phase. Also, there is a shift in the concentration, whereby erosion and deposition cycles take place at a faster rate. This is corrected in the simulation with flocculation due to it accounting for the variability in the floc size. RMSE values of suspended sediment concentration were 0.39 g/l for the simulation with flocculation, 0.69 g/l without flocculation and $w_s = 3.5$ mm/s, and 0.55 g/s for the one without flocculation and $w_s = 2.0$ mm/s.

The mean floc diameters match overall in amplitude and phase (Fig. 8, second row). The RMSE obtained for the mean floc size was 78.02 μm . The modelled settling velocity (Fig. 8, third row) shows a pattern with increasing values

for the aggregation phase, and lower values during breakage. The range of values of the settling velocity is within 1 to 2.2 mm/s, and it is smaller than conventional ranges (e.g., 2.0 to 3.5 mm/s) found in the literature of the study area (Van den Eynde 2018; Bi and Toorman 2015).

Comparison with satellite data Comparison between satellite data and model results focused exclusively on the suspended sediment concentration because it is impossible to retrieve a particle size measure from satellite data. There were seven images with low cloudiness for comparison available between 01/03/2016 and 17/05/2016. Figure 9 shows extracted time series from these images and model results at the MOW1 station. Model results, with and without flocculation, are in the same range of values of the satellite SPM data. However, they do not show the same patterns. When the model runs without flocculation, the resulting suspended sediment concentration does not display the same seasonal decreasing trend induced by the flocculation equations. The maximum RMSE, between results and satellite data at the MOW1 station, is 0.014 g/l (during 12/04/2016 11:20) for the simulation with flocculation, 0.028 g/l (during 12/03/2016 11:20) for without flocculation and $w_s = 3.5$ mm/s, and 0.056 g/l (during 12/03/2016 11:20) for the one without flocculation and $w_s = 2.0$ mm/s.

The modelled large-scale sediment concentration patterns were also assessed. Figure 10 displays a PROBA-V image and model results with timestamp 01/05/2016 11:00. There are three major plumes that the model with flocculation reproduces qualitatively well: The first over Wenduine bank, second over Paardemarkt, and the third at the Western Scheldt delta, over Vlakte van de Raan shoal. These modelled plumes have approximately the same longshore extent and shape as the observed, although they are more confined to the

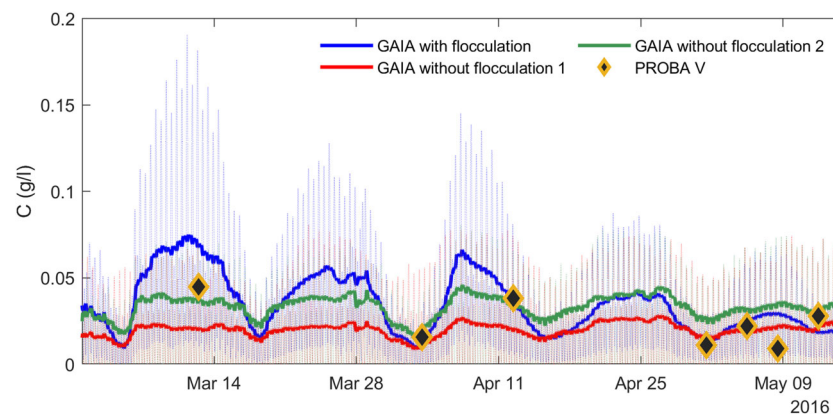
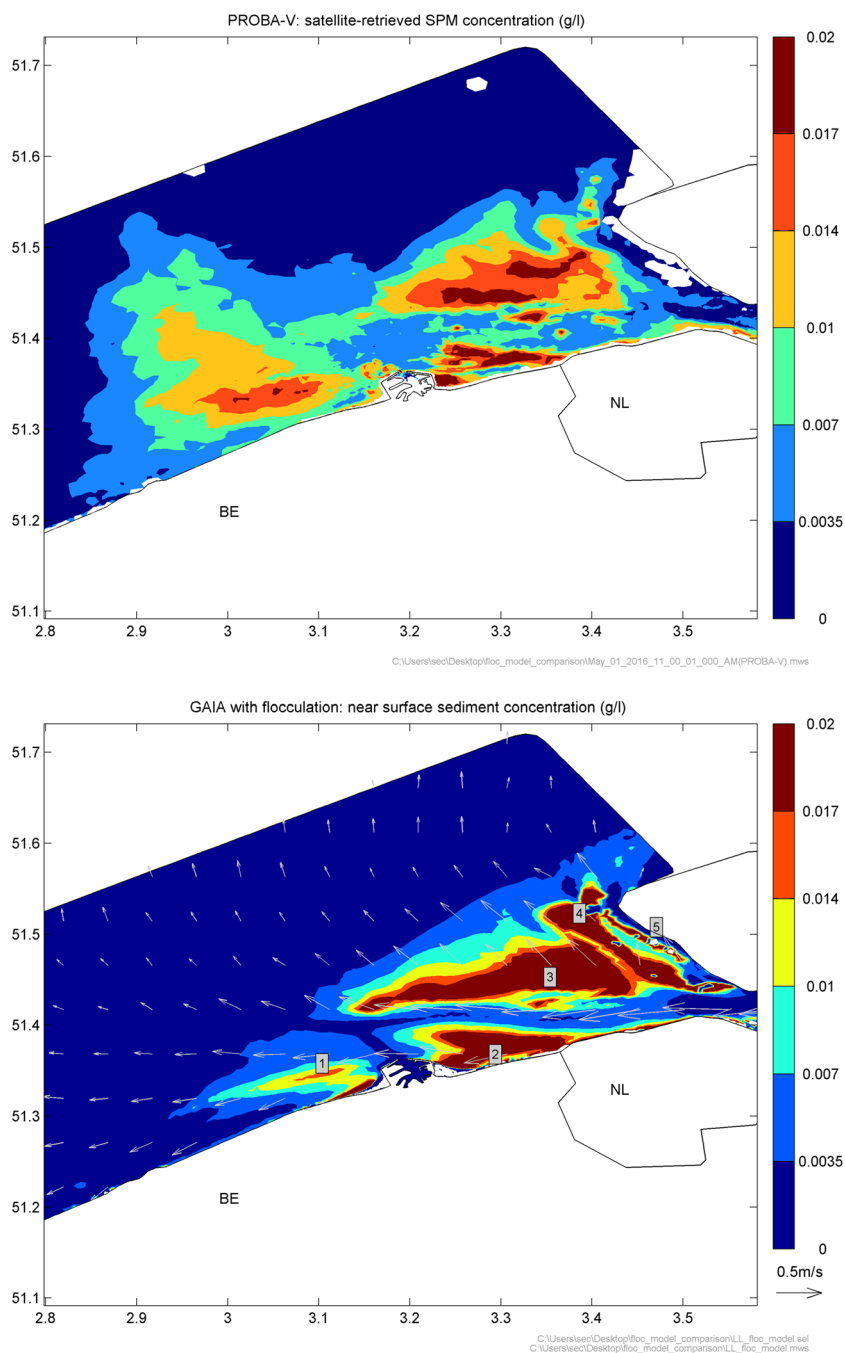


Fig. 9 PROBA-V satellite-retrieved SPM and near-surface sediment concentration retrieved from model results at the MOW1 station. The thin lines are the data extracted from GAIA, and the thick lines are the same data but filtered with a moving average window of 24 h. The

simulation “GAIA with flocculation” uses the flocculation formulation proposed in this work. “GAIA without flocculation 1” assumed a constant settling velocity of 3.5 mm/s, and “GAIA without flocculation 2” assumed a constant settling velocity of 2.0 mm/s

Fig. 10 Spatial comparison of PROBA-V satellite-retrieved SPM (top) and modelled near-surface sediment concentration achieved with the proposed flocculation setup (bottom). The timestamp is 01/05/2016 11:00. Arrows indicate the current flow velocity direction. The numbered labels over the bottom map designate known banks and shoals: 1, Wenduine bank; 2, Paardenmarkt; 3, Vlakte van de Raan; 4, Rassen; 5, Bankje van het Zouteland

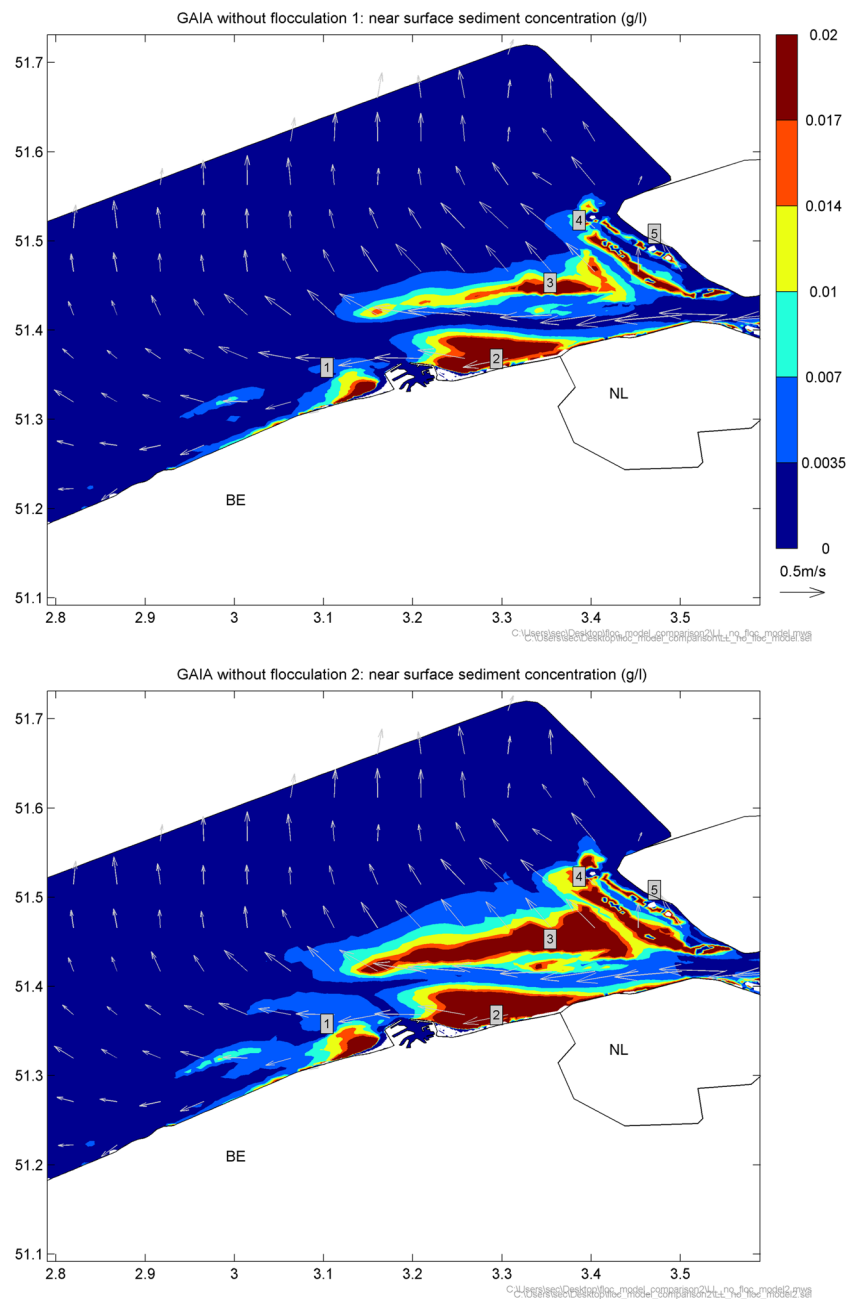


nearshore. A hypothesis that could explain the differences offshore is related with the biological processes. The satellite image was taken during spring, and in the middle of the growing season of phytoplankton Nohe et al. (2020), so the drifting plume observed off the coast may be partly made of biological SPM, which cannot be taken into account with the present model. We infer that the sediment plumes seen in Fig. 10 are mostly caused by local erosion because they overlap with the shallow and the mud-rich areas of the Western Scheldt and the Belgian Coast. Also, these plumes could

not be the result of remote transport since hydrodynamics at that time were calm, with spring tide currents up to 0.6 m/s, small wavelets (significant wave height $H_w < 0.5$ m), and light air ($U_{wind} \leq 1$ m/s).

When the flocculation equations are deactivated (Fig. 11), the sediment plumes are more localized, and the transport of sediment away from the originating shoals and banks of Paardenmarkt, Vlakte van de Raan Rassen, and Bankje van het Zouteland mostly limited. Also, different from the model with flocculation, and the satellite SPM data (Fig. 10), the

Fig. 11 Modelled near-surface sediment concentrations, without flocculation and with constant settling velocities. Top, the settling velocity was assumed 3.5 mm/s. Bottom, the settling velocity was assumed 2.0 mm/s. The timestamp is 01/05/2016 11:00. Arrows indicate the current velocity. The numbered labels over the maps designate known banks and shoals: 1, Wenduine bank; 2, Paardenmarkt; 3, Vlakte van de Raan; 4, Rassen; 5, Bankje van het Zouteland



plumes near Wenduine bank are on a narrow band on the beach. These results highlight the main limitation of conventional models where settling velocity is a constant, and that they do not properly reproduce the spatial and temporal variability of the suspension.

4 Discussion

The model presented in this work incorporates flocculation processes in the 2DH framework. Application to the Belgian

Coast indicates that it is able to reproduce the suspended sediment concentration and mean floc size dynamics of the study area with moderate success. Its main feature is that the settling velocity is a function of morphodynamics (bed shear stress and suspended sediment concentration), which is an improvement with respect to the conventional approach of using a constant settling velocity value. This can be seen in Figs. 10 and 11, where the simulation with flocculation has a better spatial agreement with the satellite-retrieved SPM. In Fig. 12, it can also be seen that the simulation with flocculation agrees more in phase and magnitude with the measurements.

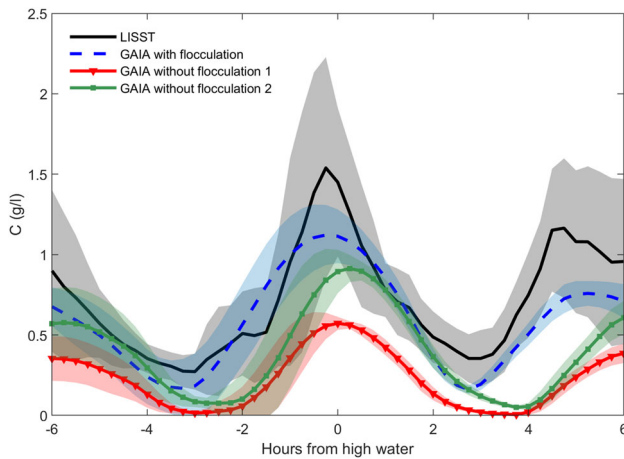


Fig. 12 Ensemble averaged concentration pattern at the MOW1 station. The black color represent LISST-measured values, the blue color represents the results of the flocculation model, and the green and red colors represent model results obtained without active flocculation and assuming constant settling velocities of 3.5 mm/s and 2 mm/s respectively. The lines are the temporal means, and the shades symbolize the standard deviation. The data belongs to the period between 20/03/2016 and 30/03/2016

The spatial patterns caused by the flocculation model are as follows: zones with the highest bed shear stresses and flow velocities have the smallest suspended flocs and lowest settling velocities. Conversely, zones with lower shear have the largest flocs and highest settling velocities. This can be observed in Fig. 13 along the navigation canal, where the flow is fast and with high shear ($\tau_b \approx 1.1$ N, $\|u\| \approx 1$ m/s), and in consequence particles are small with low settling velocity values ($50\mu\text{m}$, 0.001 m/s). In contrast, in the northwest, where flow velocity values are small ($\|u\| = 0.25$ m/s), floc size and settling velocity are the largest ($200\mu\text{m}$, 0.0026 m/s). The spatial aspect of the floc size and settling velocity is also dependent on the suspended sediment concentration. This SPM-dependence of the model may be further improved by linking empirically the coefficients k_a and k_b terms to salinity, the bed composition, organic matter content, and other aspects of the physical and biological environment which may affect electrolyte concentrations and flocculation kinetics (Fettweis and Lee 2017).

Differences between model results, and measurements and the satellite data used for model validation arise from the following limitations:

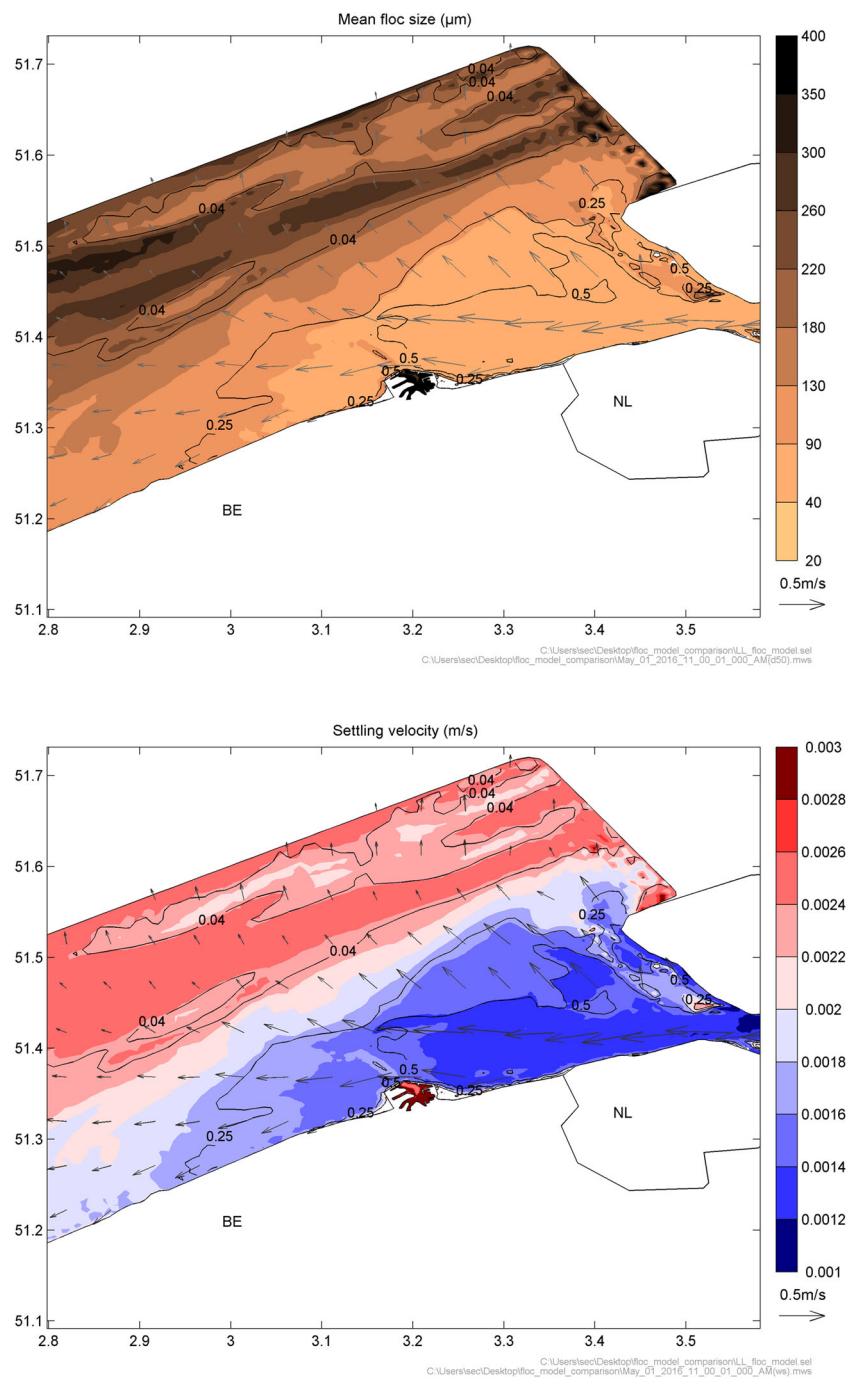
1. The floc size is multimodal, whereas the proposed model simulates the mean floc size, which makes the match of modelled results and measurements difficult to assess (Benson 2005). Moreover, Lee et al. (2012) found out, in the same study area of this work, that the estimated settling fluxes with a single discrete aggregate group had up to 45% errors against the reference settling flux of

a continuous multimodal floc size distribution (FSD). Also in the Belgian Coast, Shen et al. (2018) proved that introducing additional size groups into FSD model equations improves the prediction of settling and deposition of cohesive sediments. This explains why the presented model underestimates the low and peak values of suspended sediment concentration. Because by modelling only the mean floc size, suspended particles fall with the mean settling velocity and not the size-specific one.

2. The sediment fraction used in this work is entirely mineral; therefore, it is a simplification of the sediments found in nature. Sediments consist of inorganic and organic matter, and both groups of particles are very heterogeneous (Ho et al. 2022; Tran and Strom 2017). Also, the composition of the SPM changes with concentration; it becomes more organic when the concentration decreases. This occurs along a nearshore to offshore gradient; hence, the particles are more organic and flocculation hardly occurs in the low turbid offshore (Maerz et al. 2020; Alldredge and Silver 1988; Turner 2015). So, by not accounting for the organic part of sediments, the presented model cannot reproduce well the offshore extent of the turbidity plumes.
3. Throughout this work, we assumed a 2D depth-averaged framework. Because of this, it was necessary to then assume that the suspension followed a Rouse profile. This was later used to transfer modelled depth-averaged concentrations to the near-bed, where measurements were available, and to the near-surface, where satellite data were available for comparison. This chain of decisions is debatable since Rouse profiles are valid for steady flows, which by definition are less variegated than the combined wave-current conditions taking place at the Belgian Coast (Bolle et al. 2010; Smolders et al. 2019; Vanlede et al. 2019).
4. LISST measurements of floc size have their own uncertainties because they assume spherical particles. The LISST sensor emits a laser beam and detects light scattering by particles. The intensities of scattered light are then inverted to estimate particle size distributions assuming spherical shapes; this influences the FSD and the mean floc size estimated from it because natural flocs have irregular shapes (Shen et al. 2019; Spencer et al. 2021). Also, the presence of particles outside the size range of the LISST introduce further uncertainties in the FSD Andrews et al. (2010); Graham et al. (2012).

The above listed limitations are not unique to this work. They are commonly acknowledged in flocculation studies (Shen et al. 2019; Soulsby et al. 2013; Nohe et al. 2020; Fettweis et al. 2022), and the necessity of further knowledge to better model and measure natural floc systems is a usual con-

Fig. 13 Modelled floc size (top) and settling velocity (bottom) during 01/05/2016 11:00. Gray arrows and black contours symbolize flow velocity and bed shear stress respectively



clusion (Benson 2005; Ho et al. 2022; Spencer et al. 2021; Fettweis et al. 2019). In this context, the newly proposed flocculation formulation, and its implementation in an open-source software as TELEMAC, is a valuable step towards modelling flocs’ transport in large coastal domains. Moreover, being a 2DH model with only one additional differential Eq. 1, it has a good balance between computational time and accuracy, which is a plus with respect to more complex 3D and/or FSD models. Further developments of the proposed model are the inclusion of seasonal biological processes, and

salinity effects, which would improve results offshore and make this model applicable to estuarine waters.

5 Conclusion

A new kinetic formulation of the flocculation process, based on Winterwerp (1998) model, was implemented and assessed in a realistic application to the Belgian Coast with moderate success. Results are in the range of measured floc sizes and

suspended sediment concentrations of the study area. The model can also mimic spatial suspension patterns observed in satellite-retrieved suspended particle matter concentration maps, with modelled and observed sediment plumes matching spatially in longshore extent and location. The proposed flocculation model can therefore improve sediment transport calculations in coastal areas.

Acknowledgements This study was funded by KU Leuven, the Strategic Basic Research projects CREST and PLUXIN. These projects are funded by Flanders Innovation and Entrepreneurship (VLAIO), and for PLUXIN, also through the Flemish Blue Cluster. Scientific input from Michael Fettweis is integrated in the project MOMO funded by the Maritime Access Division of the Flemish Ministry of Mobility and Public Works. The maps and the spatial data generated during this work were processed with the MERMAID software, developed by Thomas Benson from HR Wallingford.

Author Contributions Conceptualization, E.T.; investigation, S.E., Q.B. and S.W.; writing—original draft preparation, S.E.; writing—review and editing, S.E., Q.B., E.T., J.M. and M.F.; supervision, E.T., J.M.; All authors have read and agreed to the published version of the manuscript.

Data Availability The modelling data generated during this study is available on request from the corresponding author. The measurement data are available from Royal Belgian Institute of Natural Sciences on request.

Declarations

Conflicts of interest The authors declare no conflict of interest.

Appendix A: Flocculation and sediment model calibration

A total of 19 Simulations were run with the flocculation equations activated. These simulations start on 01/03/2009 00:00 and have a duration of 45 days. The initial 25 days are considered warm-up time and discarded from any analysis. Only the remaining time interval was used.

The first simulation was called “standard”. It used the parameter values listed in in Table 2. The ensuing simulations consisted on progressive but not cumulative variations of the parameter values of the standard simulation (Table 2). The characteristic parameters of each of these simulations are listed on Table 3, column “Characteristic parameters”. The suspended sediment concentration and the mean floc size variables, at the MOW1 station, were extracted from all simulations’ results and used for sensitivity analysis and for choosing the best performing set of parameters.

The sensitivity analysis consisted of qualitative comparisons of the calibration simulations with the standard. These results can be seen in Figs. 14 and 15. The summarized patterns are listed in Table 3 (column “Response”). In general,

Table 2 Parameter values of the “standard” simulation, which was the baseline throughout the calibration process

Parameter	Value
time step (Δt)	5 s
Top layer thickness	0.1 m
Bottom layer thickness	0.3 m
Top layer mud concentration	680.0 kg/m ³
Bottom layer mud concentration	900.0 kg/m ³
E_{0s}	0.006 kg/m ² /s
E_{0m}	0.002 kg/m ² /s
$\tau_{ce,s}$	0.05 N/m ²
$\tau_{ce,m}(1)$	0.02 N/m ²
$\tau_{ce,m}(2)$	0.04 N/m ²
d_p	20 μ m
k_a	1600
k_b	30
T_r	900 s

the suspended sediment concentration is more sensible to parameters that are directly linked to sediment availability and erodibility. For example, increasing values of the bottom layer thickness and the Partheniades constants lead to larger overall concentrations. Conversely, larger values of the constant a , and lower values of the thresholds for non-cohesive and cohesive erosion, lead to lower sediment concentration values. The parameters associated with the mean floc size are less sensible regarding the suspended sediment concentration, but they do cause some important variations. Large values of the aggregation constant and the relaxation time decrease the suspended sediment concentration.

The mean floc size is more responsive to parameters linked directly to the aggregation source term. The aggregation constant plays a major role, and increasing its value causes the floc size to increase. Raising values of the relaxation time also lead to larger flocs and a slightly less peaked floc size curve. On the other hand, directly-related sediment parameters are only sensible if they cause acute decreases on the sediment concentration. That is, large values of a and low thresholds for non-cohesive and cohesive erosion cause larger floc sizes.

Regarding the critical bed shear stress, the results were not conclusive and it is difficult to assign a straightforward sensitivity to this parameter. The reason for this is that by having two vertical sediment layers, the model response to variations is consequence of the combination of critical bed shear stresses of both layers. For example, in simulations “tau ce m0015” and “tau ce s001” the critical bed shear stresses of the top layer decreased, either because the critical bed shear stress of the mud or the sand fractions were reduced. This caused the top layer to wash away and only the bottom layer remained. However, this resulted in

Table 3 Sensitivity analysis. Calibration runs are qualitatively compared with the standard simulation. The characteristic parameters are the changes relative to the standard, the arrows indicate an increase (↑) or decrease (↓) relative to the standard parameters. The response column evaluates the results relative to the standard, the arrows indicate an increase (↑) or decrease (↓) relative to the standard results

Simulation	Characteristic parameters	Response	
		C (g/l)	d (μm)
standard	—	—	—
E0S0008	$E_{0s} = 0.008 \text{ kg/m}^2/\text{s} \uparrow$	↑	↑
E0V00016	$E_{0m} = 1.6E - 4 \text{ kg/m}^2/\text{s} \downarrow$	↓	↑
Erosion law NS 05	$a = 0.5 \downarrow$	↓	↑
Erosion law NS 1 5	$a = 1.5 \uparrow$	↑	↑
tau ce m0015 ‡	$\tau_{ce,m}(1) = 0.015 \text{ N/m}^2 \downarrow$ $\tau_{ce,m}(2) = 0.025 \text{ N/m}^2 \downarrow$	—	—
tau ce m004‡	$\tau_{ce,m}(1) = 0.04 \text{ N/m}^2 \uparrow$	—	—
tau ce s001‡	$\tau_{ce,s} = 0.01 \text{ N/m}^2 \downarrow$	—	—
tshld 15 25	$f_{m,s} = 0.15 \downarrow$ $f_{m,m} = 0.25 \downarrow$	↑	↑
tshld 25 35	$f_{m,s} = 0.25 \downarrow$ $f_{m,m} = 0.35 \downarrow$	↑	↑
Top thickness 0.2	Top layer thickness = 0.2 m ↑	↓	↑
Bottom thickness 0.5	Bottom layer thickness = 0.5 m ↑	↑	↑
Tr3600	$T_r = 3600 \text{ s} \uparrow$	↓	↑
Tr3600 ka1800	$T_r = 3600 \text{ s} \uparrow$ $k_a = 1800 \uparrow$	↓	↑
Tr3600 ka1800 E0S0008	$T_r = 3600 \text{ s} \uparrow$ $k_a = 1800 \uparrow$ $E_{0s} = 8E - 3 \text{ kg/m}^2/\text{s} \uparrow$	↑	↑
Trvar3600 ka1800	$T_r = \frac{3600}{(1+100\frac{s}{m}u_*)^2} \text{ s}$ $k_a = 1800 \uparrow$	↓	↑
Trvar 900	$T_r = \frac{900}{(1+1\frac{s}{m}u_*)} \text{ s}$	↓	↑
ka2080	$k_a = 2080 \uparrow$	↓	↑
kb60	$k_b = 60 \downarrow$	-	-

‡ Non-conclusive result

lower suspended sediment concentrations because the bottom layer had larger critical bed shear stresses for the mud fraction.

The best performing simulation was chosen by ranking the RMSE of both the suspended sediment concentration and

the mean floc size, which were calculated for each simulation and with respect to measurements at the MOW1 station (see Table 4). The best simulation was “Tr3600 ka1800 E0S0008”, and its parameter values were used in Sections 3.1 and 3.2.

Fig. 14 Model calibration simulations in direct connection with the suspended sediment concentration. $\tau_{ce,m}(1)$ and $\tau_{ce,m}(2)$ are the critical bed shear stresses for erosion of mud for the top and bottom sediment layers respectively. The arrows on the figure legend indicate an increase (\uparrow) or decrease (\downarrow) in the parameter values relative to the standard simulation. LISST-measurements (black solid line) are included for reference

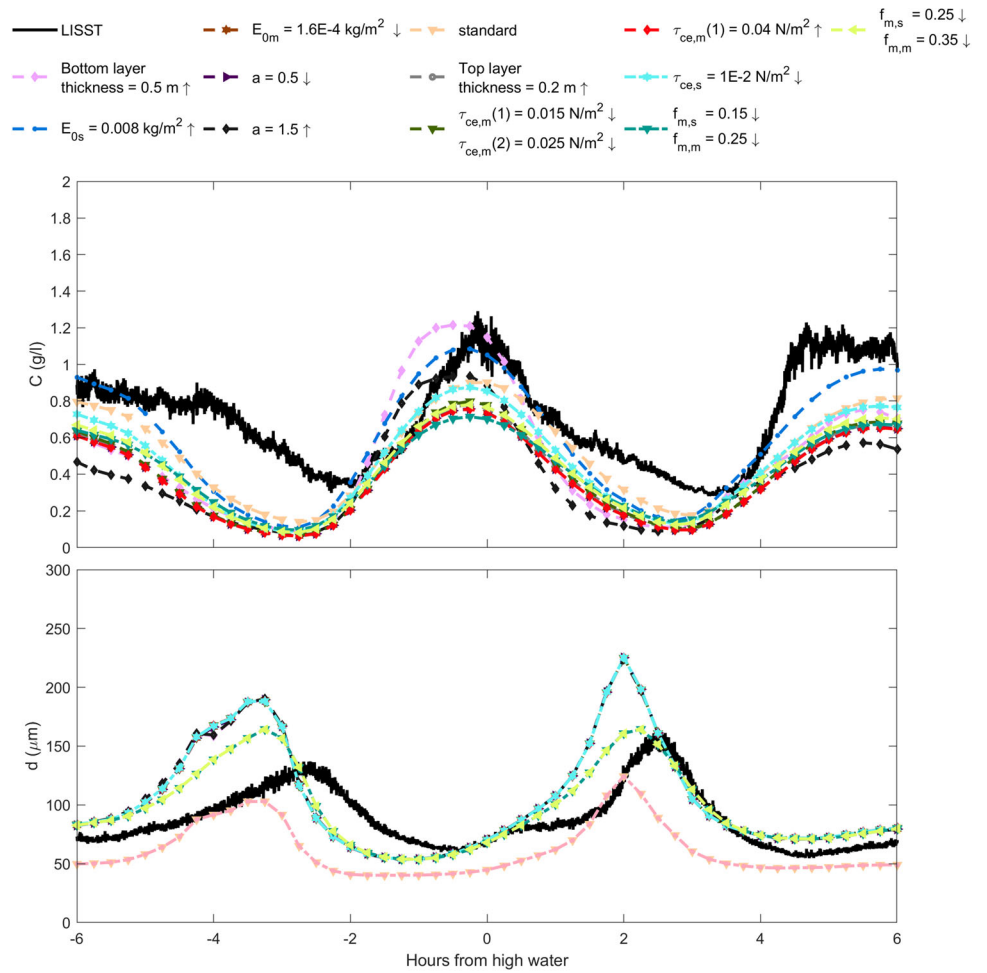


Fig. 15 Model calibration simulations in direct connection with the floc size. The arrows on the figure legend indicate an increase (↑) or decrease (↓) in the parameter values relative to the standard simulation. LISST-measurements (black solid line) are included for reference

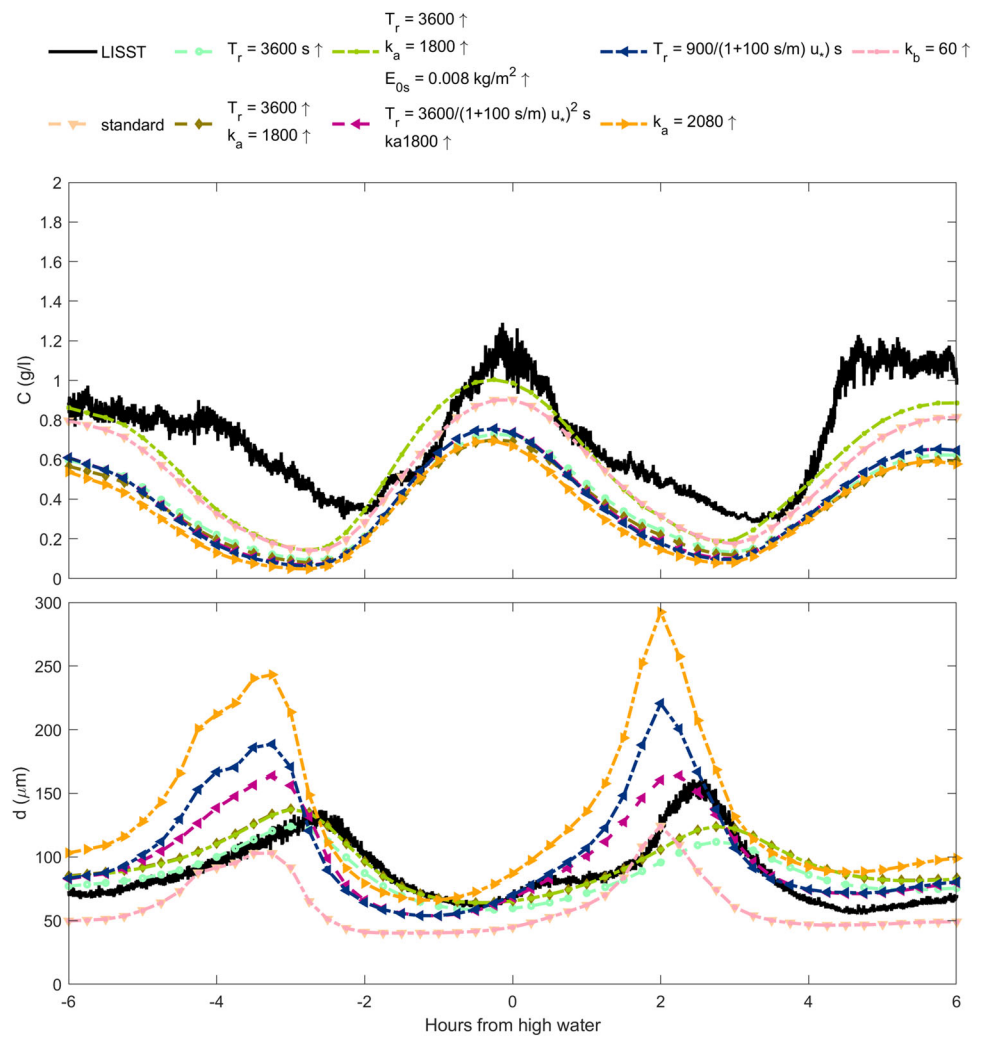


Table 4 Calibration performance in relation to measurements at the MOW1 station. The bold text highlights the best performing simulation based on the RMSE obtained both for the suspended sediment concentration and the floc size

Name	RMSE		Ranking
	\bar{C} (g/l)	d (m)	
STANDARD	0.33	29.85	2
EOS0008	0.30	46.08	5
E0V00016	0.45	45.97	12
Erosion law NS 05	0.45	45.97	11
Erosion law NS 1 5	0.46	46.14	16
tau ce m0015	0.44	46.35	13
tau ce m004	0.46	46.42	17
tau ce s001	0.38	46.43	10
tshld 15 25	0.43	32.12	6
tshld 25 35	0.42	32.11	4
Top thickness 0.2	0.45	46.43	15
Bottom thickness 0.5	0.40	46.12	8
Tr3600	0.44	19.86	3
Tr3600 ka1800	0.46	23.76	9
Tr3600 ka1800 EOS0008	0.29	23.22	1
Trvar3600 ka1800	0.45	32.08	7
Trvar 900	0.46	45.22	14
ka2080	0.50	72.34	18
kb60	0.33	29.85	2

Appendix B: Hydrodynamics-waves model assessment

The performance of the BCG model hydrodynamics are assessed for the month of March 2009. The comparison with measurements was done according to data availability, thus not all measuring stations have the same variables.

Simulated tides are in agreement with the measurements data (see Fig. 16). The maximum RMSE is 0.20 m, at the Scheur Wielingen station. Wandelaar and the A2 stations had have RMSE values of 0.17 m and 0.18 m respectively.

The flow velocities are overall on the same range of measurements, although there are noticeable phase mismatches during slack waters, both from ebb to flood and from flood to ebb tides (see Figs. 17 and 6). The RMSE at the Scheur Wielingen is 0.22 m/s, and at Bol van Heist it is 0.21 m/s (Fig. 6).

Modelled wave integrated variables are well in agreement with the measurements. The RMSE at Scheur Wielingen (Fig. 18), Wandelaar (Fig. 19) and A2 (Fig. 20) are 0.17 m, 0.15 m, and 0.16 m respectively. The mean wave period is slightly overestimated, with RMSE values of 0.64 s, 0.67 s, and 0.61 s.

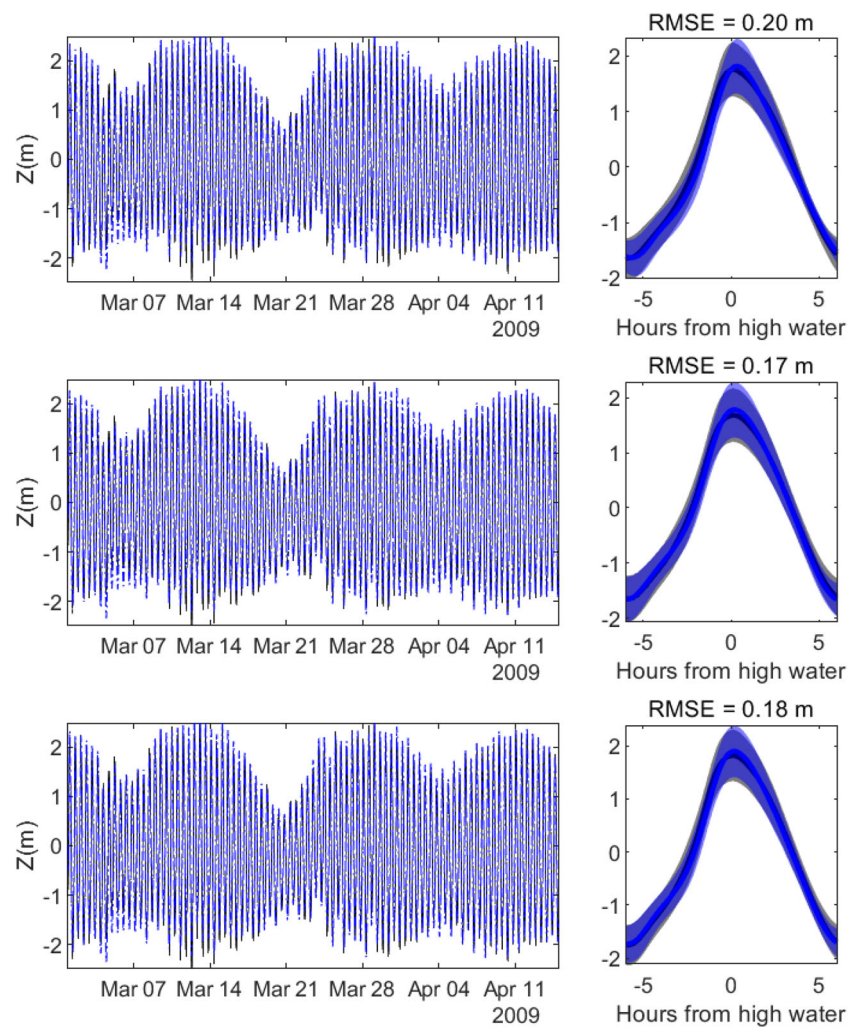


Fig. 16 Comparison of tide measurements and results of the BCG model at the Scheur Wielingen (top), Wandelaar (middle) and A2 (bottom) measuring stations. The right column shows the ensemble averages

of the times series (left column), the solid lines are temporal means and the shaded areas are the standard deviation

Fig. 17 Comparison of current velocity measurements and results of the BCG model at the Scheur Wielingen station

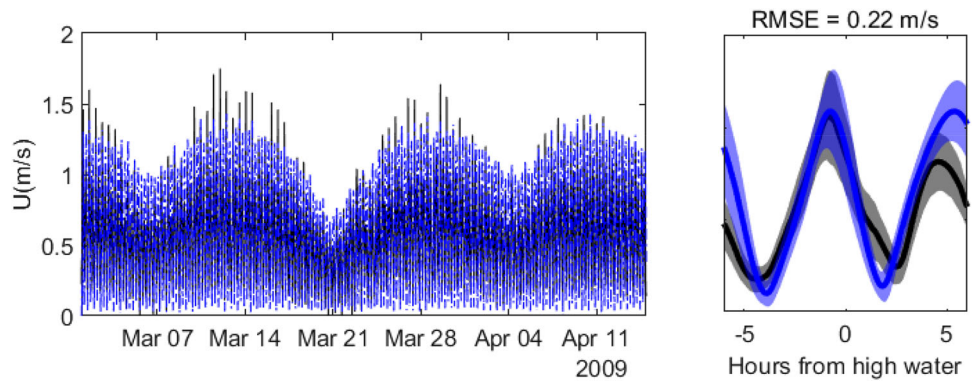


Fig. 18 Comparison of wave measurements and results of the BCG model at the Scheur Wielingen station. The black solid lines are measurements from the Flemish Banks Monitoring Network, and the blue lines are results from the BCG model

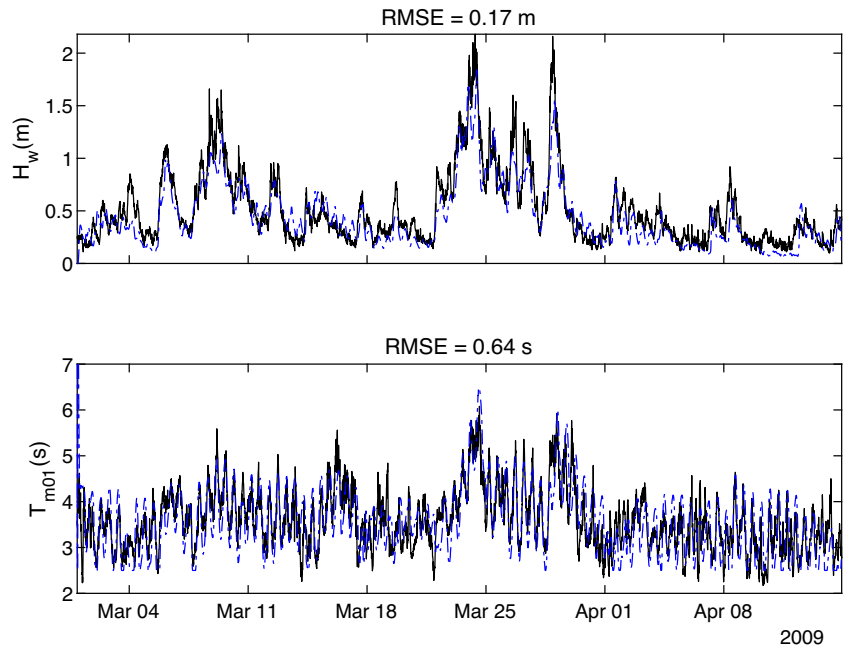


Fig. 19 Comparison of wave measurements and results of the BCG model at the Wandelaar station. The black solid lines are measurements from the Flemish Banks Monitoring Network, and the blue lines are results from the BCG model

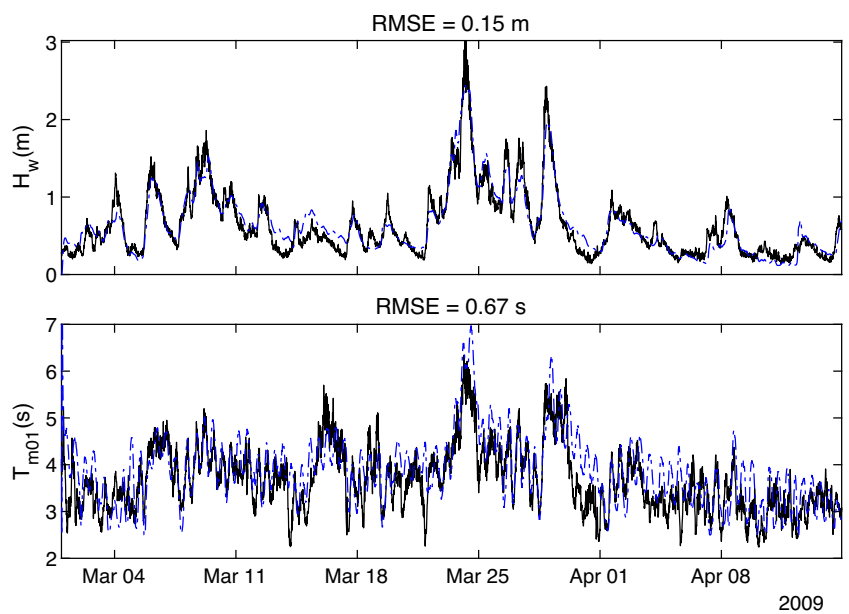
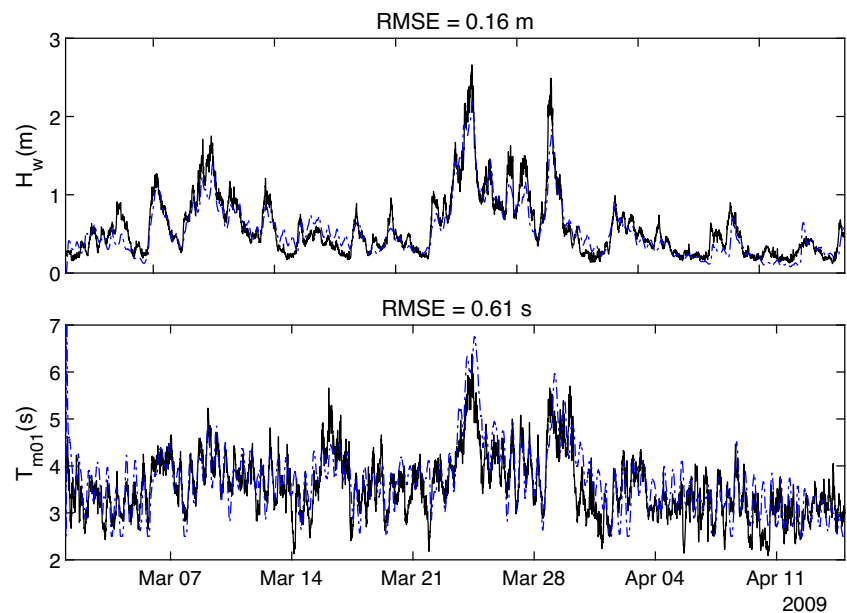


Fig. 20 Comparison of wave measurements and results of the BCG model at the A2 station. The black solid lines are measurements from the Flemish Banks Monitoring Network, and the blue lines are results from the BCG model



References

- Allredge AL, Silver MW (1988) Characteristics, dynamics and significance of marine snow. *Prog Oceanogr* 20(1):41–82. [https://doi.org/10.1016/0079-6611\(88\)90053-5](https://doi.org/10.1016/0079-6611(88)90053-5)
- AMDK (2017) Bathymetrie vooroever Vlaamse Kust. Agentschap Maritieme Dienstverlening en Kust
- Andrews S, Nover D, Schladow SG (2010) Using laser diffraction data to obtain accurate particle size distributions: the role of particle composition. *Limnology and Oceanography: Methods* 8(10):507–526. <https://doi.org/10.4319/lom.2010.8.507>
- Baeye M, Fettweis M, Voulgaris G, Van Lancker V (2011) Sediment mobility in response to tidal and wind-driven flows along the Belgian inner shelf, southern North Sea. *Ocean Dyn* 61(5):611–622. <https://doi.org/10.1007/s10236-010-0370-7>
- Baeye M, Fettweis M, Legrand S, Dupont Y, Van Lancker V (2012) Mine burial in the seabed of high-turbidity area-Findings of a first experiment. *Cont Shelf Res* 43:107–119. <https://doi.org/10.1016/j.csr.2012.05.009>
- Battjes JA, Janssen JPFM (1978) Energy Loss and Set-Up Due to Breaking of Random Waves. *Coast Eng Proc* 16:32. <https://doi.org/10.1061/9780872621909.034>
- Benoit M, Marcos F, Becq F (1997) TOMAWAC. A prediction model for offshore and nearshore storm waves
- Benson TD (2005) In: In situ particle size instrumentation for improved parameterisation and validation of estuarine sediment transport models. University of London, University College London (United Kingdom)
- Berrisford P, Dee D, Fielding K, Fuentes M, Kallberg P, Kobayashi S et al (2009) The ERA-interim archive. *ERA Rep Ser* 1:1–16
- Bi Q, Toorman EA (2015) Mixed-sediment transport modelling in Scheldt estuary with a physics-based bottom friction law. *Ocean Dyn* 65(4):555–587. <https://doi.org/10.1007/s10236-015-0816-z>
- Bi Q, Shen X, Lee BJ, Toorman E (2020) Investigation on estuarine turbidity maximum response to the change of boundary forcing using 3CPBE flocculation model. In: Online proceedings of the papers submitted to the 2020 TELEMAC-MASCARET User Conference October 2020. p 26–34
- Bolle A, Bing Wang Z, Amos C, De Ronde J (2010) The influence of changes in tidal asymmetry on residual sediment transport in the Western Scheldt. *Cont Shelf Res* 30(8):871–882. <https://doi.org/10.1016/j.csr.2010.03.001>
- Brand E, De Sloover L, De Wulf A, Montreuil AL, Vos S, Chen M (2019) Cross-shore suspended sediment transport in relation to topographic changes in the intertidal zone of a macro-tidal beach (Mariakerke, Belgium). *J Mar Sci Eng* 7(6):172
- Breugem W, Fonias E, Wang L, Bolle A, Kolokythas G, De Maerschalck B (2019) TEL2TOM: coupling TELEMAC2D and TOMAWAC on arbitrary meshes. In: XXVth TELEMAC-MASCARET User Conference, 15th to 17th October 2019. Toulouse
- Chakraborti RK, Gardner KH, Atkinson JF, Van Benschoten JE (2003) Changes in fractal dimension during aggregation. *Water Res* 37(4):873–883. [https://doi.org/10.1016/S0043-1354\(02\)00379-2](https://doi.org/10.1016/S0043-1354(02)00379-2)
- Chang TS, Joerdel O, Flemming B, Bartholomä A (2006) The role of particle aggregation/disaggregation in muddy sediment dynamics and seasonal sediment turnover in a back-barrier tidal basin, East Frisian Wadden Sea, southern North Sea. *Mar Geol* 235:49–61. <https://doi.org/10.1016/j.margeo.2006.10.004>
- Chapalain M, Verney R, Fettweis M, Jacquet M, Le Berre D, Le Hir P (2019) Investigating suspended particulate matter in coastal waters using the fractal theory. *Ocean Dyn* 69. <https://doi.org/10.1007/s10236-018-1229-6>
- Cox TJS, Maris T, Van Engeland T, Soetaert K, Meire P (2019) Critical transitions in suspended sediment dynamics in a temperate meso-tidal estuary. *Sci Rep* 9(1):12745. <https://doi.org/10.1038/s41598-019-48978-5>
- Dietrich WE (1982) Settling velocity of natural particles. *Water Resour Res* 18(6):1615–1626. <https://doi.org/10.1029/WR018i006p01615>
- Dushaw BD, Egbert GD, Worcester PF, Cornuelle BD, Howe BM, Metzger K (1997) A TOPEX/POSEIDON global tidal model (TPXO. 2) and barotropic tidal currents determined from long-range acoustic transmissions. *Progress Oceanogr* 40(1–4):337–367
- Duy Vinh V, Ouillon S, Van Uu D (2018) Estuarine Turbidity Maxima and Variations of Aggregate Parameters in the Cam-Nam Trieu Estuary, North Vietnam, in Early Wet Season. *Water* 10(1). <https://doi.org/10.3390/w10010068>
- Dyer KR (1989) Sediment processes in estuaries: Future research requirements. *J Geophys Res Oceans* 94(C10):14327–14339.

- <https://doi.org/10.1029/JC094iC10p14327>. <https://agupubs.onlinelibrary.wiley.com/doi/pdf/10.1029/JC094iC10p14327>
- Fettweis M, Baeye M (2015) Seasonal variation in concentration, size, and settling velocity of muddy marine flocs in the benthic boundary layer. *J Geophys Res Oceans* 120(8):5648–5667
- Fettweis M, Nechad B, Van den Eynde D (2007) An estimate of the suspended particulate matter (SPM) transport in the southern North Sea using SeaWiFS images, in situ measurements and numerical model results. *Cont Shelf Res* 27(10–11):1568–1583
- Fettweis M, Baeye M, Lee B, Chen P, Yu J (2012) Hydro-meteorological influences and multimodal suspended particle size distributions in the Belgian nearshore area (southern North Sea). *Geo-Mar Lett* 32(2):123–137
- Fettweis M, Baeye M, Cardoso C, Dujardin A, Lauwaert B, Van den Eynde D et al (2016) The impact of disposal of fine-grained sediments from maintenance dredging works on SPM concentration and fluid mud in and outside the harbor of Zeebrugge. *Ocean Dyn* 66(11):1497–1516
- Fettweis M, Baeye M, Francken F, Van den Eynde D, Natuur-BMM KO (2019) MONitoring en MOdelling van het cohesieve sediment-transport en evaluatie van de effecten op het mariene ecosysteem ten gevolge van bagger-en stortoperatie (MOMO). *Geosciences* 9:34
- Fettweis M, Riethmüller R, Verney R, Becker M, Backers J, Baeye M et al (2019) Uncertainties associated with in situ high-frequency long-term observations of suspended particulate matter concentration using optical and acoustic sensors. *Prog Oceanogr* 178:102162. <https://doi.org/10.1016/j.pcean.2019.102162>
- Fettweis M, Schartau M, Desmit X, Lee BJ, Terseleer N, Van der Zande D et al (2022) Organic Matter Composition of Biomineral Flocs and Its Influence on Suspended Particulate Matter Dynamics Along a Nearshore to Offshore Transect. *J Geophys Res Biogeosci* 127. <https://doi.org/10.1029/2021JG006332>
- Fettweis M, Lee BJ (2017) Spatial and Seasonal Variation of Biomineral Suspended Particulate Matter Properties in High-Turbid Nearshore and Low-Turbid Offshore Zones. *Water* 9(9). <https://doi.org/10.3390/w9090694>
- Flather RA (1979) Recent Results from a Storm Surge Prediction Scheme for the North Sea. In: Nihoul JCY, editor. *Marine Forecasting*. vol. 25 of Elsevier Oceanography Series. Elsevier, p 385–409
- Fouquet T (2020) Tomawac User Manual Version 8.1. <http://www.opentelemac.org/index.php/manuals>
- Graham G, Davies E, Nimmo-Smith W, Bowers D, Braithwaite K (2012) Interpreting LISST-100X measurements of particles with complex shape using digital in-line holography. *J Geophys Res Oceans* 117(C5)
- Hasselmann K, Barnett T, Bouws E, Carlson H, Cartwright D, Enke K et al (1973) Measurements of wind-wave growth and swell decay during the Joint North Sea Wave Project (JONSWAP). *Ergänzungsheft* 8-12
- Hasselmann S, Hasselmann K, Allender J, Barnett T (1985) Computations and parameterizations of the nonlinear energy transfer in a gravity-wave spectrum. Part II: Parameterizations of the nonlinear energy transfer for application in wave models. *J Phys Oceanogr* 15(11):1378–1391
- Hervouet JM (2000) TELEMAC modelling system: an overview. *Hydrol Process* 14(13):2209–2210
- Ho QN, Fettweis M, Spencer KL, Lee BJ (2022) Flocculation with heterogeneous composition in water environments: A review. *Water Res* 213:118147. <https://doi.org/10.1016/j.watres.2022.118147>
- Horemans DML, Dijkstra YM, Schuttelaars HM, Meire P (2020) Cox TJS. Unraveling the Essential Effects of Flocculation on Large-Scale Sediment Transport Patterns in a Tide-Dominated Estuary. *J Phys Oceanogr* 50(7):1957–1981. <https://doi.org/10.1175/JPO-D-19-0232.1>
- Hulburt HM, Katz S (1964) Some problems in particle technology: A statistical mechanical formulation. *Chem Eng Sci* 19(8):555–574. [https://doi.org/10.1016/0009-2509\(64\)85047-8](https://doi.org/10.1016/0009-2509(64)85047-8)
- Khelifa A, Hill PS (2006) Models for effective density and settling velocity of flocs. *J Hydraul Res* 44(3):390–401. <https://doi.org/10.1080/00221686.2006.9521690>
- Knaeps E, Sterckx S, Bhatia N, Bi Q, Monbaliu J, Toorman E et al (2017) Coastal turbidity monitoring using the PROBA-V satellite. *Proc Coast Dyn* 2017:1483–1494
- Komen G, Hasselmann K, Hasselmann K (1984) On the existence of a fully developed wind-sea spectrum. *J Phys Oceanogr* 14(8):1271–1285
- Komen GJ, Cavaleri L, Donelan M, Hasselmann K, Hasselmann S, Janssen P (1996) *Dynamics and modelling of ocean waves*. Cambridge University Press
- Komijani H, Ortega H (2016) Opstellen van een hydrodynamische modellen suite TELEMAC-TOMAWAC voor de Broersbank. Vlaamse Baaie - Monitoring “Broersbank”. KU Leuven
- Kranenburg C (1994) The fractal structure of cohesive sediment aggregates. *Estuar Coast Shelf Sci* 39(6):451–460. [https://doi.org/10.1016/S0272-7714\(06\)80002-8](https://doi.org/10.1016/S0272-7714(06)80002-8)
- Kuprenas R, Tran D, Strom K (2018) A Shear-Limited Flocculation Model for Dynamically Predicting Average Floc Size. *J Geophys Res Oceans* 123(9):6736–6752. <https://doi.org/10.1029/2018JC014154>
- Le Hir P, Cayocca F, Waeles B (2011) Dynamics of sand and mud mixtures: A multiprocess-based modelling strategy. *Proceedings of the 9th International Conference on Nearshore and Estuarine Cohesive Sediment Transport Processes* 31(10):S135–S149. <https://doi.org/10.1016/j.csr.2010.12.009>
- Lee BJ, Fettweis M, Toorman E, Molz FJ (2012) Multimodality of a particle size distribution of cohesive suspended particulate matters in a coastal zone. *J Geophys Res Oceans* 117(C3)
- Lee BJ, Toorman E, Molz FJ, Wang J (2011) A two-class population balance equation yielding bimodal flocculation of marine or estuarine sediments. *Water Res* 45(5):2131–2145
- Maerz J, Hofmeister R, van der Lee EM, Gräwe U, Riethmüller R, Wirtz KW (2016) Maximum sinking velocities of suspended particulate matter in a coastal transition zone. *Biogeosciences* 13(17):4863–4876. <https://doi.org/10.5194/bg-13-4863-2016>
- Maerz J, Six KD, Stemmler I, Ahmerkamp S, Ilyina T (2020) Microstructure and composition of marine aggregates as co-determinants for vertical particulate organic carbon transfer in the global ocean. *Biogeosciences* 17(7):1765–1803. <https://doi.org/10.5194/bg-17-1765-2020>
- Maggi F, Mietta F, Winterwerp JC (2007) Effect of variable fractal dimension on the floc size distribution of suspended cohesive sediment. *J Hydrol* 343(1):43–55. <https://doi.org/j.jhydrol.2007.05.035>
- Manning AJ, Dyer KR (1999) A laboratory examination of floc characteristics with regard to turbulent shearing. *Mar Geol* 160(1):147–170. [https://doi.org/10.1016/S0025-3227\(99\)00013-4](https://doi.org/10.1016/S0025-3227(99)00013-4)
- Margvelashvili N, Andrewartha J, Herzfeld M, Robson BJ, Brando VE (2013) Satellite data assimilation and estimation of a 3D coastal sediment transport model using error-subspace emulators. *Environ Model Softw* 40:191–201. <https://doi.org/j.envsoft.2012.09.009>
- Maximova T, Ides S, De Mulder T, Mostaert F et al (2009) LTV O&M thema veiligheid: deelproject 1. Verbetering hydrodynamisch NEVLA model ten behoeve van scenario-analyse, WL Rapporten, p 756
- McAnally WH, Mehta AJ (2000) Collisional aggregation of fine estuarial sediment. In: McAnally WH, Mehta AJ, editors. *Coastal and Estuarine Fine Sediment Processes*. vol. 3 of *Proceedings in Marine Science*. Elsevier, p 19–39
- Nohe A, Goffin A, Tyberghein L, Lagring R, De Cauwer K, Vyverman W et al (2020) Marked changes in diatom and dinoflagellate


- biomass, composition and seasonality in the Belgian Part of the North Sea between the 1970s and 2000s. *Sci Total Environ* 716:136316
- Press WH, Teukolsky SA, Flannery BP, Vetterling WT (1992) In: Numerical recipes in Fortran 77: volume 1, volume 1 of Fortran numerical recipes: the art of scientific computing. Cambridge University Press
- Randolph AD (1964) A population balance for countable entities. *Can J Chem Eng* 42(6):280–281. <https://doi.org/10.1002/cjce.5450420612>
- Saffman PG, Turner JS (1956) On the collision of drops in turbulent clouds. *J Fluid Mech* 1(1):16–30. <https://doi.org/10.1017/S0022112056000020>
- Shen X, Lee BJ, Fettweis M, Toorman EA (2018) A tri-modal flocculation model coupled with TELEMAC for estuarine muds both in the laboratory and in the field. *Water Res (Oxf)* 145:473–486
- Shen X, Toorman EA, Fettweis M, Lee BJ, He Q (2019) Simulating multimodal floc size distributions of suspended cohesive sediments with lognormal subordinates: Comparison with mixing jar and settling column experiments. *Coast Eng* 148:36–48. <https://doi.org/10.1016/j.coastaleng.2019.03.002>
- Shen X, Toorman EA, Lee BJ, Fettweis M (2018) Biophysical flocculation of suspended particulate matters in Belgian coastal zones. *J Hydrol* 567:238–252. <https://doi.org/j.jhydrol.2018.10.028>
- SHOM (2015) MNT topo-bathymétrie côtier, descriptif de contenu du produit externe. Service hydrographique et océanographique de la marine, France
- Smolders S, De Maerschalck B, Plancke Y, Vanlede J, Mostaert F (2019) Integraal Plan Boven-Zeeschelde: sub report 10. Scaldis Sand: a sand transport model for the Scheldt estuary. FHR Rep
- Son M, Hsu TJ (2009) The effect of variable yield strength and variable fractal dimension on flocculation of cohesive sediment. *Water Res* 43(14):3582–3592. <https://doi.org/10.1016/j.watres.2009.05.016>
- Soulsby RL, Clarke S (2005) Bed shear-stress under combined waves and currents on smooth and rough beds (TR 137). HR Wallingford. <http://eprints.hrwallingford.com/id/eprint/558>
- Soulsby RL, Manning AJ, Spearman J, Whitehouse RJS (2013) Settling velocity and mass settling flux of flocculated estuarine sediments. *Mar Geol* 339:1–12. <https://doi.org/10.1016/j.margeo.2013.04.006>
- Spencer KL, Wheatland JA, Bushby AJ, Carr SJ, Droppo IG, Manning AJ (2021) A structure-function based approach to floc hierarchy and evidence for the non-fractal nature of natural sediment flocs. *Sci Rep* 11(1):1–10
- Stephens D, Dissing M (2015) Towards Quantitative Spatial Models of Seabed Sediment Composition. *PLoS ONE* 10(11):1–23. <https://doi.org/10.1371/journal.pone.0142502>
- Tambo N, Watanabe Y (1984) Physical aspect of flocculation process: Flocculation process in a continuous flow flocculator with a back-mix flow. *Water Res* 18(6):695–707. [https://doi.org/10.1016/0043-1354\(84\)90165-9](https://doi.org/10.1016/0043-1354(84)90165-9)
- Tambo N, Watanabe Y (1979) Physical characteristics of flocs-I. The floc density function and aluminium floc. *Water Res* 13(5):409–419. [https://doi.org/10.1016/0043-1354\(79\)90033-2](https://doi.org/10.1016/0043-1354(79)90033-2)
- Tarpley DRN, Harris CK, Friedrichs CT, Sherwood CR (2019) Tidal Variation in Cohesive Sediment Distribution and Sensitivity to Flocculation and Bed Consolidation in An Idealized, Partially Mixed Estuary. *J Mar Sci Eng* 7(10). <https://doi.org/10.3390/jmse7100334>
- Tassi P, Benson T, Delinares M, Fontaine J, Huybrechts N, Kopmann R et al (2023) GAIA - a unified framework for sediment transport and bed evolution in rivers, coastal seas and transitional waters in the TELEMAC-MASCARET modelling system. *Environ Model Softw* 159:105544. <https://doi.org/10.1016/j.envsoft.2022.105544>
- Thierry S, Dick S, George S, Benoit L, Cyrille P (2019) EMODnet Bathymetry a compilation of bathymetric data in the European waters. In: OCEANS 2019-Marseille. IEEE, p 1–7
- Toorman E (1997) Mechanics of cohesive sediment transport. Proceedings on 4th Nat Congr on Applied and Theoretical Mechanics
- Toorman EA (2000) Suspension capacity of uniform shear flows. Report No. HYD/ET/00/COSINUS4. Hydraulics Laboratory, Katholieke Universiteit Leuven
- Toorman EA (2003) Validation of macroscopic modelling of particle-laden turbulent flows. In: Proceedings 6th Belgian National Congress on Theoretical and Applied Mechanics, Gent. p 26–27
- Toorman EA (2020) Background on the development and testing of a 2DH flocculation model. Hydraulics Section, Dept. of Civil Eng., KU Leuven
- Toorman EA (2022) Modification of the Dietrich (1982) formula and a new closure for the terminal settling velocity of spherical particles. *J Hydr Eng, ASCE* (submitted)
- Toorman EA, Bruens AW, Kranenburg C, Winterwerp JC (2002) Interaction of suspended cohesive sediment and turbulence. *Fine Sediment Dyn Mar Environ* 5:7–23. [https://doi.org/10.1016/S1568-2692\(02\)80005-5](https://doi.org/10.1016/S1568-2692(02)80005-5)
- Tran D, Strom K (2017) Suspended clays and silts: Are they independent or dependent fractions when it comes to settling in a turbulent suspension? *Cont Shelf Res* 138:81–94. <https://doi.org/10.1016/j.csr.2017.02.011>
- Turner JS (1973) Buoyancy effects in fluids. Cambridge University Press, Cambridge, Cambridge monographs on mechanics and applied mathematics
- Turner JT (2015) Zooplankton fecal pellets, marine snow, phytodetritus and the ocean's biological pump. *Prog Oceanogr* 130:205–248. <https://doi.org/10.1016/j.pocean.2014.08.005>
- Van den Eynde L (2018) Modelling of suspended matter for the Belgian coastal zone and the Scheldt estuary by means of PROBA-V remote sensing data. Dept. of Civil Engineering, KU Leuven
- van Leussen W (2011) Macroflocs, fine-grained sediment transports and their longitudinal variations in the Ems Estuary. *Ocean Dyn* 61(2–3):387–401
- Vanlede J, Dujardin A, Fettweis M, Hoestenbergh T, Martens C (2019) Mud dynamics in the Port of Zeebrugge. *Ocean Dyn* 69. <https://doi.org/10.1007/s10236-019-01273-3>
- von Smoluchowski M (1917) Mathematical theory of the kinetics of the coagulation of colloidal solutions. *Z Phys Chem* 92:129–168
- Waeles B, Le Hir P, Lesueur P, Delsinne N (2007) Modelling sand/mud transport and morphodynamics in the Seine river mouth (France): an attempt using a process-based approach. *Hydrobiologia* 588(1):69–82. <https://doi.org/10.1007/s10750-007-0653-2>
- Wang D, Zhang J, He X, Chu D, Lv X, Wang YP et al (2018) Parameter estimation for a cohesive sediment transport model by assimilating satellite observations in the Hangzhou Bay: Temporal variations and spatial distributions. *Ocean Model* 121:34–48. <https://doi.org/10.1016/j.ocemod.2017.11.007>
- Wang D, Zhang J, Mao X, Bian C, Zhou Z (2020) Simultaneously assimilating multi-source observations into a three-dimensional suspended cohesive sediment transport model by the adjoint method in the Bohai Sea. *Estuar Coast Shelf Sci* 241:106809. <https://doi.org/j.ecss.2020.106809>
- Weitz DA, Oliveria M (1984) Fractal Structures Formed by Kinetic Aggregation of Aqueous Gold Colloids. *Phys Rev Lett* 52:1433–1436. <https://doi.org/10.1103/PhysRevLett.52.1433>
- Winterwerp JC (1998) A simple model for turbulence induced flocculation of cohesive sediment. *J Hydraul Res* 36(3):309–326. <https://doi.org/10.1080/00221689809498621>
- Winterwerp JC (2002) On the flocculation and settling velocity of estuarine mud. *Cont Shelf Res* 22(9):1339–1360. [https://doi.org/10.1016/S0278-4343\(02\)00010-9](https://doi.org/10.1016/S0278-4343(02)00010-9)

- Zhang Y, Ren J, Zhang W (2020) Flocculation under the control of shear, concentration and stratification during tidal cycles. *J Hydrol* 586:124908. <https://doi.org/10.1016/j.jhydrol.2020.124908>
- Zhang Q, Escobar S, Toorman E, Monbaliu J (2020) Two-dimensional computations of Stokes drift and undertow at the near coast region. In: Online proceedings of the papers submitted to the 2020 TELEMAC-MASCARET User Conference October 2020. p 159–164

Publisher's Note Springer Nature remains neutral with regard to jurisdictional claims in published maps and institutional affiliations.

Springer Nature or its licensor (e.g. a society or other partner) holds exclusive rights to this article under a publishing agreement with the author(s) or other rightsholder(s); author self-archiving of the accepted manuscript version of this article is solely governed by the terms of such publishing agreement and applicable law.

Authors and Affiliations

Sebastian Escobar^{1,2}  · Qilong Bi^{1,3} · Michael Fettweis⁴ · Samor Wongsoredjo¹ · Jaak Monbaliu¹ · Erik Toorman¹

Qilong Bi
qilong.bi@deltares.nl

Michael Fettweis
mfettweis@naturalsciences.be

Samor Wongsoredjo
samor.wongsoredjo@kuleuven.be

Jaak Monbaliu
jaak.monbaliu@kuleuven.be

Erik Toorman
erik.toorman@kuleuven.be

¹ Hydraulics Laboratory, Department of Civil Engineering, KU Leuven, Kasteelpark Arenberg 40, Box 2448, Leuven 3001, Belgium

² HR Wallingford, Howbery Park, Wallingford OX10 8BA, United Kingdom

³ Department of Ecosystems & Sediment Dynamics, Deltares, P.O. Box 177, Delft 2600, MH, The Netherlands

⁴ Royal Belgian Institute of Natural Sciences, Vautier Street 29, Brussels 1000, Belgium